IEEE Access
Multidisciplinary ⋮ Rapid Review ⋮ Open Access Journal

Received December 18, 2019, accepted January 1, 2020, date of publication January 17, 2020, date of current version January 27, 2020.

Digital Object Identifier 10.1109/ACCESS.2020.2967178

Speckle Noise Reduction in Ultrasound Images for Improving the Metrological Evaluation of Biomedical Applications: An Overview

CARLOS A. DUARTE-SALAZAR[1], ANDRÉS EDUARDO CASTRO-OSPINA[1], MIGUEL A. BECERRA[2], AND EDILSON DELGADO-TREJOS[3], (Member, IEEE)

[1]MIRP Lab–Parque i, Instituto Tecnológico Metropolitano (ITM), Medellin 050026, Colombia
[2]Institucion Universitaria Pascual Bravo, Medellin 050034, Colombia
[3]CM&P Research Group, AMYSOD Lab–Parque i, Instituto Tecnológico Metropolitano (ITM), Medellin 050026, Colombia

Corresponding author: Andrés Eduardo Castro-Ospina (andrescastro@itm.edu.co)

This work was supported by the Instituto Tecnologico Metropolitano ITM of Medellin-Colombia under Project P17202.

ABSTRACT In recent years, many studies have examined filters for eliminating or reducing speckle noise, which is inherent to ultrasound images, in order to improve the metrological evaluation of their biomedical applications. In the case of medical ultrasound images, said noise can produce uncertainty in the diagnosis because details, such as limits and edges, should be preserved. Most algorithms can eliminate speckle noise, but they do not consider the conservation of these details. This paper describes, in detail, 27 techniques that mainly focus on the smoothing or elimination of speckle noise in medical ultrasound images. The aim of this study is to highlight the importance of improving said smoothing and elimination, which are directly related to several processes (such as the detection of regions of interest) described in other articles examined in this study. Furthermore, the description of this collection of techniques facilitates the implementation of evaluations and research with a more specific scope. This study initially covers several classical methods, such as spatial filtering, diffusion filtering, and wavelet filtering. Subsequently, it describes recent techniques in the field of machine learning focused on deep learning, which are not yet well known but greatly relevant, along with some modern and hybrid models in the field of speckle-noise filtering. Finally, five Full-Reference (FR) distortion metrics, common in filter evaluation processes, are detailed along with a compensation methodology between FR and Non-Reference (NR) metrics, which can generate greater certainty in the classification of the filters by considering the information of their behavior in terms of perceptual quality provided by NR metrics.

INDEX TERMS Diffusion filtering, image pre-processing, metrological evaluation, spatial filtering, speckle noise, ultrasound images, wavelet filtering.

I. INTRODUCTION

The metrological evaluation of biomedical equipment, in terms of patient safety, is important in order to avoid adverse events. Of particular interest in this review are ultrasound (US) images, which have become widely-used tools for clinical diagnosis and therapeutic procedures due to their non-invasive nature, absence of ionizing radiation, affordability, and real-time evaluation [1]. Thus, they are key in multiple medical fields such as cardiology, urology, obstetrics, and gynecology. Furthermore, they are commonly used to generate vascular imagery of internal structures in the abdominal area in order to guide surgical procedures [2]. However, US images intrinsically present speckle noise, which is a consequence of the principle of image formation, due to the interference of coherent constructive and destructive energies of scattered echoes [3], [4]. This phenomenon produces a degradation of the resolution, makes extracting significant information from US images contaminated with speckle noise a very complicated process, and negatively affects the processing tasks (i.e., segmentation, feature extraction, recording, and classification). Therefore, reducing noise in US medical images is an important step that has become a pre-processing requirement in order to conduct better analyses and diagnoses

The associate editor coordinating the review of this manuscript and approving it for publication was Tomasz Trzcinski.

in many applications (such as the visualization of body organs and object detection), without affecting critical diagnostic features in the image. However, removing speckle noise from US medical images poses a challenge because said noise cannot be uniformly modeled and is tissue-dependent, which makes its reduction even more complicated [1], [5], [6].

A considerable number of studies of varying relevance have focused on removing or smoothing speckle noise for biomedical applications. Some of them are reviews that gather and describe different approaches, while others seek to comparatively determine their advantages and limitations in a well-controlled experimental system, with the aim of conducting successful metrological evaluations. The latter is the case of the review in [7], which is a comparative study into noise elimination methods based on wavelet filters depending on different threshold values applied to US images. In their review, Mateo and Fernandez-Caballero investigated and listed some of the most widely used techniques for smoothing or removing speckle noise from US images [8]. In [9], the authors reviewed the most commonly used techniques in the literature for reducing speckle noise, but they mainly focused on echocardiographic US images. These techniques are described in detail and compared with each other applying specific criteria such as speckle noise reduction in US images, conservation of local features, and contrast ratio, among others. Rosa and Moteiro [1] analyzed the development of speckle-noise filters in US images after they identified that, in [9], the speckle noise used to contaminate the simulated images was not consistent with the predominant noise in real US images. Therefore, they used the program Field II [10] to conduct a more realistic simulation of speckle noise, thus generating B-mode (two-dimensional) US images. More recently, a study briefly reviewed filtering techniques for US images and later compared them with the method proposed therein [11].

This paper presents an overview of the concept of speckle noise in US images and the most common and important filtering techniques, along with a general discussion of their biomedical applications. Additionally, it includes some recent techniques in the field of machine intelligence that, although not yet well known, have become more relevant, as well as some modern and hybrid modalities in the field of speckle noise filtering in US images. It also presents a formal description of these methods, in order to enable the development of applications with a suitable metrological approach, detailing some common metrics in the filter evaluation process. Finally, a compensation methodology between FR and NR measurements is discussed, which enables a more detailed comparison of the implemented filters.

II. SPECKLE NOISE

In US images, speckle noise presents a multiplicative behavior strongly correlated with non-Gaussian statistics. It multiplies into the underlying US signal reflected by the tissue, thus being directly proportional to the local gray-level in that area. Therefore, speckle noise is dependent on image data, producing quality deterioration in the form of contrast reduction, blurry details, and local pseudo features [12]. The presence of speckle noise is intrinsic to US images [1], and it can be mathematically modeled through statistical distributions for multiplicative scattering [6]. As a result, traditional methods for image analysis based on the Gaussian distribution (e.g., filtering and segmentation) are not sufficient [12].

A. MODELING

In order to facilitate US image pre-processing, some studies have focused on mathematically modeling the behavior of speckle noise for multiplicative scattering [13]. The latter initially depends on the way the echo envelope signal (detected by the receiving device for US image formation) is represented, and it is defined as a reflection of the US waves that are transmitted into a human body [6]. In general, the final echo signal that is obtained is comprised of two elements: the useful signal (which is reflected by the human body) and the noise (which can be classified into two components: multiplicative and additive noise) [14], [15].

$$f(x,y) = g(x,y)\, n(x,y) + w(x,y), \quad (x,y) \in Z^2 \tag{1}$$

where $n(x,y)$ and $w(x,y)$ represent the components of the multiplicative and additive noise, respectively; (x,y), the spatial coordinates in two dimensions; and $g(x,y)$ and $f(x,y)$, the original and observed signal, respectively. Because the effect of additive noise on electrocardiograms is considerably less pronounced than that of multiplicative noise [15], model (1) can be approximated by (2).

$$f(x,y) = g(x,y)\, n(x,y), \quad (x,y) \in Z^2 \tag{2}$$

The statistical description of speckle noise $n(x,y)$ generally depends on the composition and type of tissue or US imaging system [16]. The Rayleigh distribution is commonly used to model such noise, which can be identified when the resolution cell comprises a relatively large number of independent scatterers, normally more than 10. For that reason, the amplitude of the image is said to follow the Rayleigh distribution [17]. Based on the Signal-to-Noise Ratio (SNR), two types of representation can be defined: high SNR, which is usually modeled by a Rician distribution [18], and low SNR, modeled by a K- or Nakagami distribution [19]. Moreover, the generalized gamma distribution introduced in [20] is presented in Equation (3). Said formulation is attractive because it contains several commonly used distributions that can be expressed by varying parameters in the model, such as $\alpha > 0$, a scalar parameter; $\gamma > 0$ y $\upsilon > 0$, shape parameters; and $\Gamma(\cdot)$, the gamma function. The Probability Density Function (PDF) is

$$f_N(n;\alpha,\upsilon,\gamma) = \frac{\gamma n^{\gamma\upsilon-1}}{\alpha^{\gamma\upsilon}\Gamma(\upsilon)} \exp\left\{-\left(\frac{n}{\alpha}\right)^{\gamma}\right\}. \tag{3}$$

The PDF, in (3), can represent different distributions by varying parameters υ and γ, which are frequently used in

speckle noise reduction processing. For a Rayleigh distribution (RL), $\upsilon = 1$ and $\gamma = 2$; for a Nakagamai distribution, $\gamma = 2$; and, for a Weibull distribution [21], $\upsilon = 1$. In the case of the Rayleigh distribution, n, which can also be expressed as $f(p)$, is the pixel intensity of an image at position n, and α is the form parameter of f_N related to the mean of the distribution given by $\mu = \alpha\sqrt{\frac{\pi}{2}}$. Additionally, given a spatial neighborhood of pixels with a uniform intensity $f(p)$, α can be calculated using the Maximum Likelihood Estimation (MLE) [22], [23], which is defined for Rayleigh functions as

$$\widehat{\alpha} = \sqrt{\frac{1}{2N}\sum_{q\in\Omega} f(q)^2}. \tag{4}$$

Many commercial US imaging systems are forced to compress the detected echo envelope signal using a logarithmic transformation due to their limited display range [16], [24]. For this reason, Equation (2) becomes (5), and it is simplified in (6).

$$log\left(f\left(x,y\right)\right) = log\left(g\left(x,y\right)\right) + log\left(n\left(x,y\right)\right) \tag{5}$$

$$f\left(x,y\right) = g\left(x,y\right) + n\left(x,y\right), \quad (x,y) \in Z^2 \tag{6}$$

Thus, the logarithmic transformation turns the multiplicative model of speckle noise into an additive one, which enables the application of filters designed for additive noises. However, the nonlinearity of the algorithm alters the statistics of US images and increases weak backscattering, which is why the analysis of log-compressed speckle noise is complicated [25]. Nevertheless, speckle noise $n\left(x,y\right)$ before the log-compression can be modeled by a Rayleigh distribution, and, afterward, it can be approximated to Gaussian noise [6].

B. SPECKLE NOISE REDUCTION

The presence of speckle noise in medical US images has been determined to be the cause of an eightfold reduction in the detection of injuries since 1986 [26]. Likewise, the accuracy of human interpretation and automated diagnostic functions has been affected by speckle noise [16]. In [27], it is demonstrated that reducing speckle noise improves segmentation processes. However, filtering speckle noise from sequences of images or video clips still poses a problem: most models developed for video filtering are focused on additive noise. Therefore, a multiplicative model for video footage should be created.

Several techniques have been developed in the field of US image or video pre-processing to reduce speckle noise adopting different methods, which can be classified into five categories considering their principle of analysis: Dynamic Analysis, Time-Frequency, Modern Techniques, Hybrid Techniques (HT) y Machine Learning-Based Techniques.

III. DYNAMIC ANALYSIS-BASED TECHNIQUES: ANISOTROPIC DIFFUSION

The reduction of speckle noise in echocardiograms in order to improve the detection of heart structures is an important challenge due to the difficulty in completing the process without negatively affecting the information detailed in the image. Some authors have proposed the use of techniques for smoothing images, such as Content-Unaware Smoothing (CUS) and Content-Aware Smoothing (CAS) methods [28]. CUS is the simplest, most common approach and is usually implemented with the two-dimensional Gaussian filter; however, it eliminates the imperfections in the image at the expense of blurring the edges. CAS comprises a set of techniques that adjust the behavior based on local features; one of the most relevant is Anisotropic Diffusion (AD), which has gained increasing visibility. Nevertheless, compared to linear smoothing methods, in the literature CAS has had a limited impact in edge detection [29].

Diffusion takes place in accordance with the Partial Differential Equation (PDE) (7) described in [9], which details the dissemination of particles from high-concentration regions into their low-concentration counterparts. A linear version of the diffusion equation is used to describe the distribution of heat in a region over time. A variety of techniques that adopt nonlinear diffusion methods to treat noise in US images have been reported in the literature. For instance, in 1990, Perona and Malik [30] proposed anisotropic diffusion as a generalization of the diffusion equation to reduce noise in US images, which was shown in [7], by smoothing homogeneous areas while preserving the edges. Nevertheless, its effect on images that present multiplicative noise (such as speckle noise) was less satisfactory.

$$\begin{aligned} \frac{\partial f\left(x,y;t\right)}{\partial\left(t\right)} &= \nabla\cdot\left[c\left(\left|\nabla f_\sigma\left(x,y;t\right)\right|\right)\cdot\nabla f\left(x,y;t\right)\right] \\ f\left(x,y;0\right) &= f_0\left(x,y\right) \end{aligned} \tag{7}$$

where $\nabla\cdot()$ represents the divergence operator, ∇ is the gradient, $|\cdot|$ indicates the magnitude, and $c\left(|\nabla f_\sigma\left(x,y;t\right)|\right)$ contains function $c(\cdot)$ that controls the diffusion levels at each position in the image with f_σ, which represents a smoothed version of f.

Later, in 2002, Yongjian and Acton [31] developed a diffusion approach to eliminate speckle noise using statistical methods, thus creating the Speckle Reducing Anisotropic Diffusion (SRAD) filter. The latter also uses the diffusion PDE but with the diffusivity function $c\left(\cdot\right)$ comprised of Instantaneous Coefficients of Variation (ICOV), q, which are used as signal/edge discriminators. Afterward, Fernández and López [32] proposed a filter that outperforms SRAD, Detail Preserving Anisotropic Diffusion (DPAD), as can be seen in (8), considering the largest neighborhoods to more accurately estimate the components of the ICOV. Additionally, the approach of estimating the scale function of the speckle $q_0\left(t\right)$, which is the diffusion threshold that controls

the level of smoothing as the median of $[q(x, y; t)]$, produces computational savings because it requires fewer calculations than SRAD [33].

$$c\left[q(x, y, t), q_0\right] = \frac{1 + 1/q^2(x, y, t)}{1 + 1/q_0^2(t)} \tag{8}$$

Weickert [34] introduced the function of the diffusion tensor with Coherence-Enhancing Diffusion (CED), allowing the smoothing level to vary directionally. This diffusion tensor is based on the T-structure tensor, which represents the gradient of image $\nabla f\left(f_x, f_y\right)$ as in (9), being f_x, f_y the gradients in directions x and y. CED employs two smoothing stages. First, the noise fluctuation in the observed image is reduced by a variance Gaussian kernel σ^2, denoted as K_σ; likewise, $f_\sigma = K_\sigma * f$, where $*$ represents the convolution. The second stage is a second level of smoothing, where the structure tensor is formed as T_ρ (9).

$$\begin{aligned} A)\ T &= \left(\nabla f \otimes \nabla f^T\right) = \begin{pmatrix} f_x^2 & f_{xy} \\ f_{xy} & f_y^2 \end{pmatrix} \\ B)\ T_\rho &= K_\rho * \left(\nabla f_\sigma \otimes \nabla f_\sigma^T\right) = \begin{pmatrix} T_{11} & T_{12} \\ T_{21} & T_{22} \end{pmatrix} \end{aligned} \tag{9}$$

where the eigenvalues of $T_\rho(\mu_1, \mu_2)$ are ordered in such a way that $\mu_1 \geq \mu_2$ and the corresponding eigenvectors $(\vec{\omega}_1, \vec{\omega}_2)$ provide the direction of the gradient and the edge, respectively. The CED process is described by the following differential equation.

$$\frac{\partial f(x, y; t)}{\partial t} = \nabla \cdot [D \nabla f(x, y; t)] \tag{10}$$

where D is the diffusion matrix constructed with the same eigenvectors of T_ρ and eigenvalues (λ_1, λ_2) [9].

Abd-Elmoniem *et al.* [16] proposed Nonlinear Coherent Diffusion (NCD) (11) for discriminating different speckle levels based on the similarity of fully-developed speckle, i.e., the regions in the image that closely resemble fully-developed speckle are filtered with a median filter, while those that are different remain unchanged.

$$J_\rho = K_\rho * \left(\nabla f \nabla f^T\right) = \begin{pmatrix} K_\rho * f_x^2 & K_\rho * f_{xy} \\ K_\rho * f_{xy} & K_\rho * f_y^2 \end{pmatrix} \tag{11}$$

NCD is not based on the initial state of (9.B); for that reason, the structure matrix represents the information of the gradient from all the details in the image, even the smallest ones. Therefore, the eigendecomposition of J_ρ produces the eigenvectors $(\vec{\omega}_1, \vec{\omega}_2)$, which provide the direction of the gradient and the contour. In the same way as CED, the diffusion process is given by PDE (10), with D as the diffusion tensor constructed to have the same eigenvectors as J_ρ and the eigenvalues (λ_1, λ_2) [9].

Krissian*et al.* [35] proposed an SRAD method extended to a matrix diffusion scheme, called Oriented Speckle Reducing Anisotropic Diffusion (OSRAD), which enables adaptable diffusion to vary in resistance to the direction of the contour and the curvature. This technique implements the improvements of the DPAD method, such as the use of a larger window to estimate $q(x, y; t)$ and its median, to obtain $q_0(t)$. The SRAD method is extended to a matrix scheme by finding the local directions of the gradient and the curvature, which can be done by using the Hessian matrix, as in [36]; however, in that study, the authors use the structure tensor, similar to CED and NCD methods. Recently, other authors [37] proposed the use of a semi-adaptive threshold (SAT) in the diffusion coefficient function to better protect the detailed information and improve noise reduction. First they applied a pre-reduction with the local difference value method, in order to distinguish between corrupted and noise-free pixels, thus replacing those contaminated with speckle with pixels that had been pre-filtered with a Gaussian filter. After this, the Perona-Malik (PM) anisotropic diffusion model was implemented with a SAT based on the local gradient over the function of the diffusion coefficient, which indicates that the gradient value of the corrupt pixels is introduced in the threshold, resulting in greater diffusion in smooth areas and less diffusion in boundary regions. Additional studies into Magnetic Resonance Imaging (MRI) and US images, such as [38]–[40], have been recently published. They focus on finding the optimal value of the Threshold of Gradient Modulus (TGM), which is one of the most important operating parameters of the AD filter, because fitting the TGM to its optimal value by trial and error is subjective, difficult, and time-consuming [38].

IV. TECHNIQUES BASED ON TIME-FREQUENCY ANALYSIS

This section describes the methods that work in the wavelet domain along with spatial domain techniques. Said spatial domain is associated with adaptive filters that are commonly applied to Synthetic Aperture Radar (SAR) images.

A. WAVELET-BASED METHODS

Wavelet filtering can be carried out by adjusting to zero the coefficients of the decomposition levels that represent noise and maintaining the coefficients that contain information about the features of the image. This method is called Wavelet Shrinkage (WS), and it uses a threshold to determine which coefficients need to be eliminated. WS is effective in reducing additive noise in images. For images affected by multiplicative noise, other authors [41] introduced a speckle noise reduction method using a threshold of the wavelet coefficients of the log-transformed image, as shown in (6). Since the logarithm is a homeomorphic transformation, multiplicative noise becomes additive noise; thus, the Daubechies wavelet transform with 4 levels of decomposition was implemented to remove speckle while preserving the resolution of the original image.

Other studies have sought to improve the thresholding rule in US images. Such is the case of the speckle-noise reduction method reported by Zong *et al.* [15], which is based on the model in (5). They studied hard and soft thresholding methods to develop a combined approach in order to reduce speckle and improve the features of the image by calculating

the Wavelet Discrete Transform (DWT) formulated in [42], which describes the j levels of $f(m, n)$, as in (12).

$$W\left[f\left(m,n\right)\right]=\left\{\left(W_j^d\left[f\left(m,n\right)\right]\right)_{1\leq j\leq J}^{d=1,2},\ S_J\left[f\left(m,n\right)\right]\right\} \quad (12)$$

where $W_j^d[f(m, n)]$ is a wavelet coefficient in the scale of 2^j; $f(m, n)$, the position; and d, the spatial orientation ($d = 1$ for horizontal and $d = 2$ for vertical). The coefficients of approximation to the closest scale K are indicated by $S_J[f(m, n)]$ [9], [15].

In [43], a Bayesian formulation was adopted to efficiently find a threshold for WS; it was based on the observation of the wavelet coefficients in a subband of the log-transformed images that can be modeled using the generalized Gaussian distribution, and such threshold was estimated by minimizing the Bayes risk function. A different approach was proposed in [44] with the Nonlinear Multiscale Wavelet Diffusion (NMWD), a technique that iteratively filters speckle utilizing a nonlinear diffusivity function over the wavelet coefficients [2]. When wavelet-based signal/noise discrimination is combined with anisotropic diffusion, however, the gradient cannot always accurately separate the image from the noise in US images because the variations caused by speckle noise can be higher than those of the underlying image [9]. In [45], the authors presented a technique that can be applied to different and unknown types of image noise: the Generalized Likelihood Method (GLM). The GLM employs a preliminary detection of the wavelet coefficients that represent the features of interest in order to empirically estimate the conditional of the coefficients of the Probability Density Function (PDF) given the useful features and the background noise, instead of being based on previous knowledge of the exact distribution of the noise, which, in general, enables the estimation of the PDF of the noise-free wavelet coefficients based on the noisy histogram. Recently, other authors [46] presented an algorithm that has a double filter bank structure, which consists of two decomposition stages. The first one involves the decomposition of third-level wavelet packets, which establishes that the best bases are selected using Adaptative Wavelet Packet Transform (AWPT), referring to the work of Esakkirajan *et al.* [47]. Subsequently, Singular Value Decomposition (SVD) is applied to all the subbands, except for the low frequencies because they are preserved as such by the AWPT; thus, high-frequency subbands that present high singular values are selected. During the second stage, 3 levels of the iterated Directional Filter Bank (IDFB) are applied to each selected subband; subsequently, the modified NeighShrink rule is applied to the resulting cells to reduce the high-frequency noise of each additional subband. Finally, the highest frequency subbands are reconstructed based on the directional cells using the inverse IDFB. This is followed by the reconstruction of the images combining the low-frequency subband with its reconstructed high-frequency counterparts.

B. SAR-BASED METHODS

Synthetic Aperture Radar (SAR) is a coherent satellite positioning radar system for image creation that uses the relative movement between the sensor and the target area [48]. Its products suffer from a degradation similar to that in US images, and, for that reason, the methods proposed to reduce speckle in SAR images are also applicable to US medical images [9]. Lee's filter [49] features an image processing algorithm based on the considerations of the local statistics of the images, and it has the particularity of processing each pixel separately without waiting for its neighbor pixels to be processed. That structure makes it naturally adequate for parallel processing in order to improve contrast and noise filtering. The basic assumption of said technique is that the mean of the sample and the variance of a pixel are equal to the local mean and the variance of all the pixels within a fixed range that surrounds them. In addition, this technique is an extension to treat multiplicative and additive noise filtering based on the simple multiplicative model in [50], approaching (2), and using a linear model to obtain the estimation of the signal $\widehat{R}$ (13) described in [9].

$$\widehat{R}\left(x,y\right)=f\left(x,y\right)+\overline{f\left(x,y\right)}\left\{1-W\left(x,y\right)\right\} \quad (13)$$

with $W(x, y)$ as the weighting function given by:

$$W\left(x,y\right)=1-C_n^2/C_I^2 \quad (14)$$

where C_I is the coefficient of variation of the noisy image and C_n, the coefficient of variation of the noise.

Another technique that can be applied in this case is the filter proposed by Kuan *et al.* [51], which is obtained by transforming (2) into a formulation of additive noise dependent on the signal, instead of the linear approximation used in Lee's filter. The same general form of Lee's filter [52] is used, but with a weighting function given by (15) and described in [9].

$$W\left(x,y\right)=\frac{1-C_n^2/C_I^2}{1-C_n^2} \quad (15)$$

Frost *et al.* [53] proposed a filter that estimates the noise-free image using the convolution of the image observed with a spatially variable kernel expressed as $\widehat{R}\left(x,y\right) = f\left(x,y\right) * m\left(x,y\right)$). Kernel $m\left(x,y\right)$, centered on the pixel at position (x_0, y_0), is given as:

$$m\left(x,y\right)=K_1\boldsymbol{e}^{\left(-kC_n^2(x_0,y_0)|x,y|\right)} \quad (16)$$

where parameter K controls the attenuation rate, $|x, y|$ represents the distance from each pixel in the window to (x_0, y_0), and K_1 is a normalization constant. Lopes *et al.* [54] expanded the approaches of Lee and Frost et al. by adapting local heterogeneity and, based on the C_I, dividing the image into three different filtering regions using two additional thresholds.

V. MODERN TECHNIQUES

Some modern techniques have been proposed in recent years. For instance, Tay *et al.* [55] presented a Squeeze Box Filter (SBF) to iteratively remove local extrema, which are

assumed to be atypical data, in order to later replace them with the local mean; thus, regions are smoothed while the edges that define them are preserved. Their work was initially projected over an ideal squared noise-free signal, and they start by defining J as the original signal and $\tilde{J} = J$. In order to ensure that the filter acts on the local regions of the current image or signal $\tilde{J}$, white Gaussian noise with a little variation is initially and regularly added, as shown in (17).

$$\tilde{J}(n,m) = \tilde{J}(n,m) + \eta(n,m) \tag{17}$$

Subsequently, at iteration i, the first step is to determine the set of locations of the local maxima and minima of $\tilde{J}$. The location of the local extrema is defined by the set

$$\begin{aligned} E = &\left\{ \overrightarrow{n} \,|\tilde{J}_{i-1}(\overrightarrow{n}) \text{ satisfies condition 1 or 2} \right\} \\ &Condition\ 1 : \tilde{J}_{i-1}(\overrightarrow{n}) > \tilde{J}_{i-1}(\overrightarrow{m}) \\ &Condition\ 2 : \tilde{J}_{i-1}(\overrightarrow{n}) < \tilde{J}_{i-1}(\overrightarrow{m}) \end{aligned} \tag{18}$$

where $m = n \pm 1$ for 1D signals and $\overrightarrow{m} = (m_1, m_2 = (n_1 \pm 1, n_2 \pm 1))$ for 2D images.

After the local extrema have been identified, each one of them is replaced with the local mean taken from neighbor samples without including local maxima and minima (19). For each $(n,m) \in E$. As a result, the local variance of the signal or image is gradually reduced, and atypical data are eliminated.

$$\tilde{J}\left(\overrightarrow{n}\right) = \frac{1}{|N|} \sum_{\overrightarrow{s} \in N} \tilde{J}_{i-1}(\overrightarrow{s}) \tag{19}$$

where N are some local neighbors of $\overrightarrow{n}$ and $|N|$ is the cardinality of set N, with $\overrightarrow{n} \notin N$. And, when convergence is achieved,

$$\sum_{\forall \overrightarrow{n}} |\tilde{J}_{i-1}(\overrightarrow{n}) - \tilde{J}_i(\overrightarrow{n})| < \epsilon. \tag{20}$$

If the total number of iterations is not reached at some predefined $\epsilon > 0$, the process is repeated from the addition of Gaussian noise or the location of the local extrema, depending on whether more low-variance zero-mean noise should be added or not. If the total number of iterations is reached, the filtering process stops [55], [56].

Balocco [23] proposed an automatic Speckle Reducing Bilateral Filter (SRBF) for US images by incorporating speckle-noise statistics into the weighting scheme based on the Rayleigh noise distribution, which was integrated into the framework of a basic filter by Aysal [57] and the Classical Bilateral Filter (CBF) initially proposed by Tomasi and Manduchi [58]. The latter does not consider the nature of the image and it works by replacing the value (or weight) of the central pixel in the window with the weighted average of its neighbors. The calculation of the weights depends on spatial distances and intensity (21)-(22).

$$h(p) = \Gamma^{-1}(p) \int_{\Omega(p)} f(\xi) c(\xi, p)\, s(f(\xi), f(p)) d\xi \tag{21}$$

with a normalization factor of:

$$\Gamma(p) = \int_{\Omega(p)} c(\xi, p)\, s(f(\xi), f(p)) d\xi \tag{22}$$

where f is the original image; h, the filtered image; $\Omega(p)$, the spatial neighbors of a generic pixel p; and ξ, the integration variable that represents the coordinate of pixels in Ω. The classical framework of the bilateral filter defines c and s as unbiased isotropic Gaussian functions.

$$c(\xi, p) = \exp\left(-\frac{\|p - \xi\|}{2\sigma_c^2}\right) \tag{23}$$

$$s(f(\xi), f(p)) = \exp\left(-\frac{(f(p) - f(\xi))^2}{2\sigma_s^2}\right) \tag{24}$$

where σ_c represents the Gaussian standard deviation in the spatial support and σ_s is the standard deviation in the range domain. These two parameters control the weight decrease in the spatial domain and intensity, respectively, which indicates that the selection of such parameters is important to eliminate noise from images, considering that high values produce an excessive smoothing of the image, blurring fine structures and edges in the image, while low values produce poor noise elimination results [5]. Therefore, in (23), they spatially weight the Euclidian distance between p and ξ, while in (24) they work in the intensity domain [23], [58]. Nevertheless, regarding US images, it is not valid to assume a zero mean in the noise statistics, which is typical of the classical bilateral filter and anisotropic filtering frameworks. For that reason, the Bilateral Filter (BF) has been expanded to US images [23], integrating the statistics of speckle noise into the filter and redesigning the function s as the probability that $f(p)$ belongs to the Rayleigh distribution (3) that generated $f(\xi)$. Given a local neighborhood around p characterized by a Rayleigh distribution $RL_p(\alpha)$, the probability of the intensity of the central pixel $f(p)$ that belongs to $RL_x(\alpha)$ can be expressed as

$$p[f(p) \in RL_{\xi}(\alpha)] = \frac{f(p)}{\widehat{\alpha}_{\xi}^2} \exp\left(-\frac{f(p)^2}{2\widehat{\alpha}_{\xi}^2}\right). \tag{25}$$

In [23], $\widehat{\alpha}$ is approximated by the value of pixel $f(\xi)$, and $s(f(\xi), f(p))$ is established the same as $p[f(p) \in RL_{\xi}(\alpha)]$. This is because the BF calculates function s in all the pixels in the spatial neighborhood, and the errors of the Rayleigh estimation are averaged converging to the local MLE. Therefore, when the central pixel in a neighborhood x and its neighbors belong to a similar Rayleigh distribution, function s produces high values and promotes smoothing. Otherwise, s produces a low value when there is a contour, thus preserving the edges.

The same as the BF, some techniques propose to adapt the Non-Local Means (NLM) method to the speckle noise model. Although the BF and the methods above are based on the paradigm of local adaptive recovery [59], in which local pixels are compared, the NLM adopts a new nonlocal recovery paradigm based on patches and proposed by Buades *et al.* [60]. According to the latter, the pixels in the

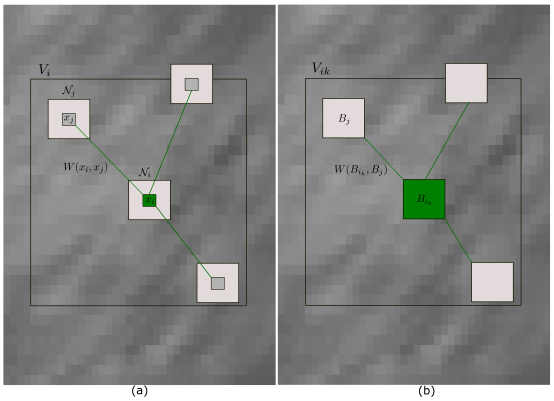

FIGURE 1. a) Classical NLM filter pixel, b) Blockwise NLM filter [62].

image and the weight of each pixel are averaged based on the distance of the surrounding patches (26), thus replacing the local comparison of pixels with the non-local comparison of patches [61]. This paradigm enables the NLM to achieve a more robust noise elimination performance than the BF [58]. For that reason, different authors [61] proposed the Optimized Bayesian NLM (OBNLM), which is an adaptation that employs a Bayesian formulation to define a Pearson's distance in order to compare patches of the damaged image with speckle noise and makes the most of the blockwise implementation of the NLM method for the algorithm acceleration.

$$NL(f)(x_i) = \sum_{x_j \in \Omega^{dim}} \mathcal{W}(x_i, x_j) f(x_j) \tag{26}$$

where $f = (f(x_i))_{x_i \in \Omega^{dim}}$ is initially considered as the noisy image defined over a limited domain $\Omega^{dim} \subset \mathbb{R}_+$ (which is usually a rectangle of a $\Omega^{dim}|$ size); $f(x_i) \in \mathbb{R}_+$ is the intensity of the noise observed in pixel$x_i \in \Omega^{dim}$; *dim*, the dimensions of the image ($dim = 2$ or $dim = 3$ for 2D and 3D, respectively); and $\mathcal{W}(x_i, x_j)$, the weight assigned to value $f(x_j)$ to restore pixel (x_i), i.e., the weight evaluates the similarity between the intensities of the local neighborhoods (patches) $\mathcal{N}_i$ and $\mathcal{N}_j$ centered at pixels x_i and x_j, such that $\mathcal{W}(x_i, x_j) \in [0, 1]$ and $\sum_{x_j \in \Omega^{dim}} \mathcal{W}(x_i, x_j) = 1$ (Figure 1).

In the classical method, for practical and computational reasons, the number of pixels taken into account in the weighted average is restricted to a neighborhood and not the entire image, i.e., a "search volume" V_i of a size $(2M+1)^{dim}$ centered at the current pixel x_i. For each pixel $x_j \in V_i$, the Euclidian distance is calculated with Gaussian weighting $\|\cdot\|^2_{2,a}$ between the two patches of image $\mathbf{f}(\mathcal{N}_j)$ and $\mathbf{f}(\mathcal{N}_i)$, as seen in [60], where the central pixels in the patch contribute more to the distance than pixels in the periphery. This measurement is the traditional L_2-norm convoluted with a Gaussian kernel of standard deviation a. For that reason, the weights in (26) are calculated as follows.

$$\mathcal{W}(x_i, x_j) = \frac{1}{Z_i} \exp - \frac{\left\|\mathbf{f}(\mathcal{N}_i) - \mathbf{f}(\mathcal{N}_j)\right\|^2_{2,a}}{h^2} \tag{27}$$

where Z_i is a normalization constant that ensures that $\sum_{x_j \in \Omega^{dim}} \mathcal{W}(x_i, x_j) = 1$, and h acts as a smoothed parameter that controls the decrease in the exponential function.

However, when an L_2-norm between two patches is considered, a white Gaussian additive noise model is assumed. For that reason, some authors have proposed to focus on multiplicative speckle noise [61]. This approach is initially derived from a blockwise NLM formulation proposed in [62], (28), to reduce the computational load.

$$\begin{aligned} NL(u)(B_i) &= \sum_{B_j \in \Delta^{i_k}} \mathcal{W}(B_i, B_j)\mathbf{u}(B_j) \text{ with } \mathcal{W}(B_i, B_j) \\ &= \frac{1}{Z_i} \exp - \frac{\left\|\mathbf{f}(B_{i_k}) - \mathbf{f}(B_j)\right\|^2_{2,a}}{h^2} \end{aligned} \tag{28}$$

where $\mathbf{f}(B_i) = (f^1 B_i, \ldots, f^P B_i)^T$ is a patch of image that gathers the intensities of block (B_i), and $\left\|\mathbf{f}(B_{i_k}) - \mathbf{f}(B_j)\right\| = \sum_{p=1}^{P} (f^p(B_i) - f^p(B_j))^2$.

Afterward, said authors equal the Bayesian formulation to the estimator of conventional measures, where estimator $\widehat{\mathrm{v}}(B_{i_k}))$ of block B_{i_k} can be defined as

$$\widehat{\mathrm{v}}(B_{i_k}) = \frac{\sum_{J=1}^{|\Delta_{i_k}} \mathbf{f}(B_{i_k}) p(\mathbf{f}(B_{i_k})|\mathbf{f}(B_j))}{\sum_{J=1}^{|\Delta_{i_k}} p(\mathbf{f}(B_{i_k})|\mathbf{f}(B_j))} \tag{29}$$

where $p(\mathbf{f}(B_{i_k})|\mathbf{f}(B_j))$ denotes the Probability Density Function (PDF) of $\mathbf{f}(B_{i_k})$ conditioned to $\mathbf{f}(B_j)$. The probability, in the case of a white Gaussian additive noise $p(\mathbf{f}(B_{i_k})|\mathbf{f}(B_j))$, is proportional to $e^{-\left\|\mathbf{f}(B_{i_k}) - \mathbf{f}(B_j)\right\|^2_{2,a}/h^2}$.

To study multiplicative noise, e.g., speckle, models such as those presented in Section 2.1 should be taken into account. However, the noise model used for OBNLM is different because, when the complex formation process of US images is considered, some of the factors mentioned in [61] come to light and tend to demonstrate that the Rayleigh model used for Radio Frequency signals is not adequate to analyze log-compressed US images. Regardless, in the wavelet domain for noise elimination [16], [63], [64], multiplicative speckle noise is supposedly transformed into additive Gaussian noise employing log-compression. Recent studies into US images also demonstrate that the distribution of noise is satisfactorily approximated through a gamma distribution [65] or a Fisher-Tippett distribution [66]. Therefore, we adopted Loupas noise model [67], which has been successfully used in many studies [68]–[70], because it is more flexible and less restrictive than the usual Radio Frequency model; furthermore, it can capture reliable image statistics since factor γ depends on the US devices and the additional processing related to image formation. Furthermore, Loupas et al. demonstrated that, with $\gamma = 0.5$, the model fits the data better than multiplicative or Rayleigh models.

$$u(x) = v(x) + v^{\gamma}(x)\eta(x) \tag{30}$$

where $v(x)$ is the original image; $u(x)$, the observed image; and $\eta(x) \sim \mathcal{N}(0, \sigma^2)$, zero-mean Gaussian noise.

Then, considering the Bayesian formulation (29) and Loupas noise model (30), assuming $u(x)v(x) \sim \mathcal{N}(v(x), v(x)^{2\gamma}\sigma^2)$ for each pixel, Pearson's distance is introduced to compare the patches in the image.

$$dp(\mathbf{u}(B_i), \mathbf{u}(B_j)) = \sum_{p=1}^{P} \frac{(u^p(B_i) - u^p(B_j))^2}{(u^p)^{2\gamma}(B_j)} \tag{31}$$

Thus, $dp(\mathbf{u}(B_i), \mathbf{u}(B_j))$ is defined as Pearson's distance with $\gamma = 0.5$, which substitutes the usual L_2-norm. However, the OBNLM filter presents certain difficulties because it can effectively remove the noise from the images that contain fine structural details, but it produces an excessive smoothing of the edges and the textures in the picture [5]. Other authors [71] presented a measurement similar to the OBNLM within the same Bayesian framework they used to define the Euclidian distance implementing the model in Equation (30). Their purpose was to iteratively refine weights $\mathcal{W}^i(x, y)$ in a low-dimension subspace thorough a Principal Component Analysis (PCA) in order to improve accuracy and reduce computational complexity. Nevertheless, they were not able to preserve low-contrast features because they are usually very blurry due to the great similarity between the patches surrounding said features and the patch centered at the speckle noise. Furthermore, finding similar pixels over the entire US image takes considerable time [56].

VI. HYBRID TECHNIQUES (HT)

Some authors have proposed the integration of several techniques to improve speckle-noise reduction in US images. Such integration processes depend entirely on the type of techniques selected to create the hybrid method.

On the one hand, a hybrid algorithm as a sequential process that comprises three noniterative stages is proposed in [5]. During the first stage, a *Guided Filter* (GF) is applied to eliminate the effect of speckle noise, which was initially proposed by He *et al.* [72] to exploit local second-order statistics. Therefore, Choi and Jeong [73] decided to efficiently use the advantages of the GF focused on speckle reduction in a wavelet-based algorithm. The main assumption of the GF [72] is that guide I and filter output Q are related through a local linear model; as a consequence, in [5], Q is assumed as a linear transform of I in a window ω_k centered at pixel k.

$$Q_i = a_k f_i + b_k. \ \forall_i \in \omega_k \tag{32}$$

where (a_k, b_k) are some linear coefficients assumed to be constant in ω_k. With this linear model, the objective is to ensure that Q has an edge only if f has an edge because $\nabla Q = a\nabla f$. Hence, to determine the linear coefficients, we should find a solution to (32) that minimizes the difference between Q and the filter input p, more specifically, the cost function (33) [5].

$$E(a_k, b_k) = \sum_{i\in\omega_k} (a_k f_i + b_k - p_i)^2 + \varepsilon a_k^2 \tag{33}$$

where ε is a regularization parameter that prevents a_k from being excessively large.

$$a_k = \frac{\frac{1}{|\omega|}\sum_{i\in\omega_k}(f_i p_i - \mu_k \bar{p}_k)}{\sigma_k^2 + \varepsilon} \tag{34}$$

$$b_k = \bar{p}_k - \mu_k a_k \tag{35}$$

where μ_k and σ_k^2 represent the mean and variance of f in ω_k, respectively; $|\omega|$ is the number of pixels in ω_k; and $\bar{p}_k$ denotes the mean of p in ω_k, given as $\bar{p}_k = \frac{1}{|\omega|}\sum_{i\in\omega_k} p_i$. Thus, (a_k, b_k) are calculated for all the patches of ω_k in the image and the filter output, as shown in (36).

$$Q_i = \frac{1}{|\omega|} \sum_{k:i\in\omega_k} a_k f_i + b_k = \bar{a}_i f_i + \bar{b}_i \tag{36}$$

with $\bar{a}_i = \frac{1}{|\omega|}\sum_{k\in\omega_i} a_k$ and $\bar{b}_i = \frac{1}{|\omega|}\sum_{k\in\omega_i} b_k$.

In the second stage, a Speckle Reducing Bilateral Filter (SRBF) is applied over the image pre-filtered by the GF using weights based on the distance of the squared chord, which employs the speckle noise model in (30) with $\gamma = 0.5$. In the last stage, to preserve the edges and details of the fine structures, this method proposes a filter that consists in NLM with weights $\mathcal{W}(x_i, x_j)$ calculated through the Rotationally Invariant Bilateral (RIB) similarity measure reported in [74]. The objective is to prevent patches with similar structures to the reference patch, but with different orientations, from influencing the average; for that reason, in [5], $\mathcal{W}(x_i, x_j)$ for 2D images is defined as follows.

$$\mathcal{W}_{RIB}(x_i, x_j) = \exp\left(-\frac{1}{2}\frac{\left(\mathbf{u}\left(\mathcal{N}_i\right) - \mathbf{u}\left(\mathcal{N}_j\right)\right)^2 + 2\left(\mu_{\mathcal{N}_i} - \mu_{\mathcal{N}_j}\right)^2}{r^2}\right) \tag{37}$$

where $\mu_{\mathcal{N}_i}$ and $\mu_{\mathcal{N}_j}$ represent the mean of the reference patch and the patch that is processed within the search area Ω^{dim}, respectively, and "r" is the smoothing parameter. The local means $\mu_{\mathcal{N}_i}$ and $\mu_{\mathcal{N}_j}$ are calculated once for the entire image using small neighborhoods, approximately 5×5, to avoid excessive smoothing of singular structures in the image, and they are stored in a matrix the same size as the image. Moreover, the NLM filter with RIB (RIBNLM) presents low complexity and produces an adequate weighting of patches with similar structures but different orientations in relation to the reference patch.

On the other hand, a hybrid method that combines local statistics with the NLM filter is proposed in [75]. Such method consists in estimating noise using local statistics over local patches to change the way the coefficients of the weights in the NLM filter are calculated because the patch in the noisy image is not directly evaluated as patches are first smoothed by local statistics. The procedure of said method starts with the estimation of the noise-free image utilizing the Local Linear Minimal Mean-Squared Error (LLMMSE)

in the following way [76].

$$\hat{v}_{LLMMSE}(\mathbf{x}) = E\left[v\left(\mathbf{x}\right)\right] + \frac{\sigma_v^2\left(\mathbf{x}\right)}{\sigma_u^2\left(\mathbf{x}\right)}\left[u\left(\mathbf{x}\right) - E\left(u\left(\mathbf{x}\right)\right)\right] \quad (38)$$

Taking into account Loupas model (30), $\hat{v}_{LLMMSE}(\mathbf{x})$ is the estimation of $v\left(\mathbf{x}\right)$; $\sigma_v^2\left(\mathbf{x}\right)$ and $\sigma_u^2\left(\mathbf{x}\right)$ are the variances of $v\left(\mathbf{x}\right)$ and $u\left(\mathbf{x}\right)$, respectively; and $E\left[v\left(\mathbf{x}\right)\right]$ and $E\left[u\left(\mathbf{x}\right)\right]$ are the expectations of $v\left(\mathbf{x}\right)$ and $u\left(\mathbf{x}\right)$, respectively.

Since $\eta(x)$ is a zero-mean Gaussian noise in Equation (30), we get

$$E\left(u\left(\mathbf{x}\right)\right) = E\left[v\left(\mathbf{x}\right)\right] \quad (39)$$

Consequently, variance $\sigma_u^2\left(\mathbf{x}\right)$ can be defined as

$$\begin{aligned}\sigma_u^2(\mathbf{x}) &= E\left(u^2\left(\mathbf{x}\right)\right) - E\left(u\left(\mathbf{x}\right)\right)^2 \\ &= E\left(v\left(\mathbf{x}\right) + v^{\gamma}\left(\mathbf{x}\right)\eta\left(\mathbf{x}\right)\right)^2 - E\left(v\left(\mathbf{x}\right)\right)^2 \\ &= \sigma_v^2\left(\mathbf{x}\right) = \left(\mathbf{x}\right) + \sigma_\eta^2\left(\mathbf{x}\right)E\left(v^2\left(\mathbf{x}\right)^{2\gamma}\right) \end{aligned} \quad (40)$$

where $\sigma_\eta^2\left(\mathbf{x}\right)$ is the variance of $\eta(\mathbf{x})$.

Additionally, in [75], $\hat{v}_{LLMMSE}(\mathbf{x}))$ is revised as

$$\begin{aligned}&\hat{v}_{LLMMSE}(\mathbf{x}) \\ &= E\left(u\left(\mathbf{x}\right)\right) + \frac{\sigma_u^2(\mathbf{x}) - \sigma_\eta^2(\mathbf{x})E\left(u(\mathbf{x})\right)}{\sigma_u^2\left(\mathbf{x}\right)}\left[u\left(\mathbf{x}\right) - E\left(u\left(\mathbf{x}\right)\right)\right]\end{aligned} \quad (41)$$

where $\gamma = 0.5$.

$$\begin{aligned}&\hat{v}_{LLMMSE}(\mathbf{x}) \\ &= E\left(u\left(\mathbf{x}\right)\right) + \frac{\sigma_u^2(\mathbf{x}) - \sigma_\eta^2(\mathbf{x})E\left(u(\mathbf{x})\right)^2}{\left(1 + \sigma_\eta^2\left(\mathbf{x}\right)\right)\sigma_u^2\left(\mathbf{x}\right)}\left[u\left(\mathbf{x}\right) - E\left(u\left(\mathbf{x}\right)\right)\right]\end{aligned} \quad (42)$$

where $\gamma = 1$ and $E\left(u\left(\mathbf{x}\right)\right)$ with $\sigma_u^2\left(\mathbf{x}\right)$ are approximated by the local mean. For further information in this regard, see [75].

Afterward, the coefficients of the weights and the constant normalization are modified as follows.

$$\begin{aligned}&\mathcal{W}'(x_i, x_j) \\ &= \frac{1}{Z_i}\exp\left(-\frac{\left\|\hat{v}_{LLMMSE}\left(\mathcal{N}_i\right) - \hat{v}_{LLMMSE}\left(\mathcal{N}_j\right)\right\|_{2,a}^2}{h^2}\right)\end{aligned} \quad (43)$$

$$\begin{aligned}&Z' \\ &= \sum_{x_j \in \Omega^{dim}} \exp\left(-\frac{\left\|\hat{v}_{LLMMSE}\left(\mathcal{N}_i\right) - \hat{v}_{LLMMSE}\left(\mathcal{N}_j\right)\right\|_{2,a}^2}{h^2}\right)\end{aligned} \quad (44)$$

where h is the smoothing parameter. Therefore, NLM integrated with Local Statistics (LS) is called NLMLS:

$$NLMLS(u_i) = \sum_{x_j \in \Omega^{dim}} \mathcal{W}'(x_i, x_j)u(x_j) \quad (45)$$

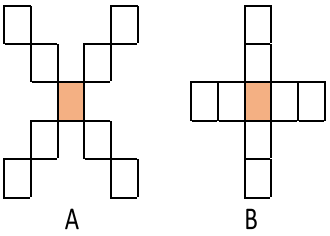

FIGURE 2. Diagram of the pixel neighborhood. A) 45° X-shaped neighborhood, B) 90° +-shaped neighborhood.

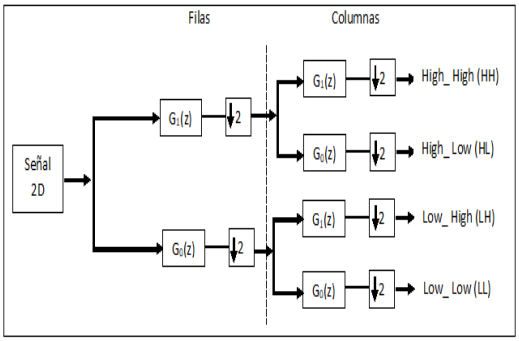

FIGURE 3. Wavelet decomposition into the 4 subbands [78], [80].

A hybrid model is also presented in [77] for reducing speckle noise. However, it is based on first-level DWT combined with a hybrid filter of median and SRAD to analyze images based on the 4 subbands produced by the wavelet decomposition (LL, LH, HL, and HH) [78], as can be seen in Figure 3. In said figure, LL is filtered by SRAD, which preserves the information of the texture. In the other three high-frequency subbands, noise is extracted through the median hybrid filter [79]. This involves an operation divided into three steps over a 5×5 neighborhood, in which pixels are classified into two groups, as shown in 2, to examine the 45° and 90° neighborhoods, including their central pixel. The three steps are described below.

1) Calculate the median (M) of the pixels marked with R (MR) in (46) including the central pixel C in a 5×5 neighborhood.

$$\begin{pmatrix} D & * & R & * & D \\ * & D & R & D & * \\ R & R & C & R & R \\ * & D & R & D & * \\ D & * & R & * & D \end{pmatrix} \quad (46)$$

2) Calculate the M of the pixels marked with D (MD) in (46), taking the central pixel into account.
3) Lastly, in (47), M is calculated with the values of MR and MD plus C.

$$M_1 = median(MR, MC, C) \quad (47)$$

where M_1 is the filter output and the new value of the central pixel.

After the four filtered subbands have been obtained, the image is reconstructed by calculating the inverse DWT

and subjecting it to a total variation (TV) filter [81], [82] to achieve better noise reduction. The TV of a signal is the measurement of how much the signal has changed within the range of values of its data. Specifically, the TV of N points in a signal $F(n)$, $1 \leq n \leq N$ is defined as follows.

$$TV(F) = \sum_{n=2}^{N} |F(n) - F(n-1)| \tag{48}$$

Given an input signal F_n, the objective of this method is to find an approximated signal G_n, which represents a TV lower than, but close to, x_n; and one of the measurements of proximity is the sum of squared errors (49).

$$E(F, G) = \frac{1}{2}\sum\nolimits_n (F_n - G_n)^2 \tag{49}$$

As a consequence, the TV approach eliminates the noise by minimizing the discrete function (50) over signal G_n.

$$E(F, G) + \lambda TV(\mathbf{G}) \tag{50}$$

where parameter λ is a positive value that specifies the fidelity weight that controls the amount of noise reduction.

By differentiating the functionality above from G_n, in the original approach a corresponding Lagrangian-Eulerian equation is derived and numerically integrated with the original signal F_n as an initial condition. Depending on the behavior of the problem, different optimization techniques can be used to minimize and find the solution to G_n; for example, in a convex function [82].

VII. MACHINE LEARNING-BASED TECHNIQUES

Recently, several authors have addressed the problem of speckle-noise reduction in US images from the field of machine learning, using new concepts of soft metrology to develop methods that enable its implementation in low-cost (portable) US equipment and real-time applications. Here we review multiple studies that have responded to that challenge.

In [83], the authors presented a method with multi-resolution Convolutional Neural Networks (CNN) within the framework of homomorphic filtering, which considers speckle noise to be multiplicative; therefore, they implemented a logarithmic transformation of the data followed by the exponentiation of the results, as explained in [84]. First, they proposed an end-to-end CNN architecture for speckle filtering in US images, thus demonstrating that their results are significantly close to those of state-of-the-art filtering algorithms, working $\times 4$ times faster on a GPU and $\times 8$-260 faster on a CPU. The training of the CNN was focused on converting regular US images into pictures similar to those of Computed Tomography (CT), which have better resolution and contrast while preserving all the relevant anatomical and pathological elements. This process was based on the use of a dataset of in-phase and quadrature (IQ) images, derived from radiofrequency (RF) pictures through frequency demodulation. It is important to note that these pictures were obtained using a fast US data simulation scheme [85] for which patches extracted from The Cancer Imaging Archive (TCIA) were employed [86]. Subsequently, the IQ data were applied some conventional speckle filters, such as TV and NLM, to use them as reference points when the network was trained and thus achieve a speckle reduction similar to said filters. Nevertheless, the main focus was to demonstrate the capacity of CNNs to reconstruct the quality of a CT based on US images, directly using patches from images in the TCIA instead of already-filtered pictures for the training. However, in practice, paired CT-US data are difficult to obtain, and a possible solution would be the development of a non-supervised/semi-supervised training framework.

In contrast, other authors [87] adopted a Deep Learning approach. They proposed a CNN architecture with modules composed of a deep residual network (ResNet) so that it could learn how to eliminate speckle using the results of classical filtering methods, thus avoiding the limiting task of fitting the parameters they require in accordance with the input datum. Their method used 380 real US images of livers collected from sources such as Medanta Hospital (in Gurgaon, India) and an open-access database (http://www.ultrasoundcases.info/Cases-Home.aspx). The images were filtered applying four different techniques: DPAD, OBNLM, Edge Aware Geometric Filtering (EAGF) [88], and Anisotropic Diffusion with Memory based on Speckle Statistics (ADMSS) [89]. As a result, they presented a first approach using the results of the 4 filters as ground truth, comparing them with the output of the CNN model in the training process, and employing the cost function of the Multiscale Structural Similarity (MS-SSIM) index [90], where the total loss was calculated as the sum of the individual losses. In their second approach, they followed the same process but, in terms of ground truths, they used the combined results of the filters concerning ADMSS to produce a better output. In order to train the CNN model, in the last experiment (compared to the previous one), they used the training dataset to generate samples of 4 different sizes: 32×32, 64×64, 96×96, and 128×128. They determined that, in a ResNet of 3×3 convolutional layers, the best performance was achieved with 64×64 samples and, in the case of 5×5 convolutional layers, with a 128×128 size.

In [91], the authors proposed an architecture based on ResNet modules as a Despeckling Residual Neural Network (DRNN) over US images to be used within the framework of the Generative Adversarial Network (GAN) as the generator model (G); in the case of the discriminator (D), they employed a CNN. The training data came from two sets of actual US images of livers of healthy subjects obtained with different equipment; one of the sets contains low-quality high-speckle (LQHS) images, while the other is comprised of images with high-contrast and much less speckle (HCLS). The DRNN, in the framework of the GAN, is trained in two steps. The first is for pretraining G and D using structural cost functions given in (51) and (52) along with synthetic data; for that purpose, they started with the HCLS set in order to simulate the speckle noise over such images (applying the method reported in [92]) and provide a reference point in the first

training process. In the second step, the two networks in the GAN framework have the same input data. To train D, they used the same loss function (52); however, the loss function to train G was combined with the discriminating model and trained with real data for speckle reduction. This combination occurs when the adversarial cost function imposed by D is combined with the structural cost function (53), as the latter acts as a regulator and it helps to produce the expected results.

$$\mathcal{L}(\theta) = L_1(\theta) + L_{Ms-SSIM}(\theta) \tag{51}$$

$$L_D(\phi) = E_x\left[-\log\left(D\left(y;\phi\right)\right)\right] + E_x[-\log(1 - D(G(x;\theta);\phi))] \tag{52}$$

where $L_1(\theta)$ is the standard cost function ℓ_1; $L_{MS-SSIM}(\theta)$ is the MS-SSIM function; and θ and ϕ represent the parameters of the G and D models, respectively.

$$\mathcal{L}(\theta) = E_x\left[-\log\left(D\left(G\left(x;\theta\right);\phi\right)\right)\right] + \lambda\mathcal{L}(\theta) \tag{53}$$

The first term in (53) is the adversarial cost function, $E[\cdot]$ represents the expectation, and $D(\cdot)$ and $G(\cdot)$ are the outputs of the discriminant and generation models, respectively, according to the input parameters. In the presence of that cost, parameter θ was optimized so that the generated image is close to HCLS images; and, in order to avoid overestimation of the features learned by D to differentiate high-quality images, the structural cost function $\mathcal{L}(\theta)$ is accompanied by parameter λ, which was used with a value of 1 in this study.

Other studies have focused on enhancing US images obtained by transmitting a single wave plane (WP) as they are low quality, in terms of resolution and contrast, compared to those obtained by applying the classical approach that uses 31 WPs. The objective of these studies is to reduce the cost and increase the speed of US image construction, which is even more necessary in ultrafast US imaging methods. Said methods have attracted the interest of the scientific community due to their high rate per frame, which has enabled a wide range of diagnostic modalities, such as elastography and functional US imaging [93]. In [94] and [95], a method based on CNN was proposed for reconstructing images from a low- to a high-quality space. Specifically in [94], the authors demonstrated the capacity of a CNN to reconstruct a high-quality image from 3 WPs with simulated and real datasets. Furthermore, an architecture inspired by the popular U-Net, which consists in a residual CNN with a coder-decoder structure, has also been reported [95]. Such a network was trained with synthetic images sourced from the PICMUS dataset in order to improve the quality of the images reconstructed from a single WP, thus enhancing the performance of ultrafast US imaging.

VIII. QUALITY METRICS

The set of quality metrics commonly implemented in metrological evaluations [96] contains FR measures that use a ground truth to produce the comparison; they include Pratt's Figure of Merit (FoM), Structural Similarity (SSIM), and Mean Squared Error (MSE). Nevertheless, in some studies, such as [9], they have been proposed along with Contrast-to-Noise Ratio (CNR) and Signal-to-Noise Ratio (SNR_A) to more thoroughly calculate and determine the effect filtering has on the quality of US images. The first three metrics above have a comparative nature, that is, between two images. In the case of simulated images, each contaminated picture, after being filtered, is compared with the ideal (noise-free) reference image. In the case of real images, the metrics are applied using the non-filtered or original image as a reference. In contrast, the CNR metric evaluates a single image, which involves its calculation in the filtered image as well as in the reference to use the difference between those two values to measure the change caused by the filter. The SNRA metric is used to measure noise reduction due to filtering.

Further, other authors confirmed the significant statistical relationship there is between the metric FoM and the evaluation, by experts, of the general quality of clinical echocardiographic videos [96]. They also found a significant relationship between the Edge Region MSE and the clarity of the critical details, as perceived by experts. As a result, successful filtering is not only based on the criterion of speckle-noise removal, particularly in images used for medical diagnosis, as reported by other authors [9] who indicate that the application of objective metrics (such as FoM and Edge MSE) can quantify other aspects of the filtering process (e.g., measuring the similarity of the edges between the filtered and the reference image). For that reason, effective filtering is closely related to the performance that can be achieved by automatic endocardium edge detection techniques in US images, thus enabling the classification of noise fluctuation as edge points [97]. CNR values show how good the methods of the filters are at increasing the contrast compared to the reference image. Finally, the measurements with low SSIM values may indicate a structural difference concerning the reference image, although the noise levels in both can be similar.

It is also essential to highlight the role that NR metrics can play in quality image evaluation because they do not require an original image to be compared to, which can facilitate this measurement process since, in many problems, the ground truth is not available, as it is common in medical imaging applications. However, in [98], the authors demonstrate the existence of a relationship between FR distortion measurements and NR perceptual quality employing a mathematical analysis. They establish that such measurements are not in agreement, that is, the lower the distortion of an algorithm, the further its distribution should be from the statistics of natural scenes, thus generating a degraded perceptual quality. They empirically demonstrate this compensation in many popular distortion measurements, including those that were considered well correlated with human perception. Therefore, in that work, they conclude that any distortion mea-

surement on its own is not adequate to evaluate image restoration methods. For that reason, they propose a methodology using NR and FR metrics to graph each algorithm in a perception-distortion plane to produce a comparison that provides more information about restoration or filtering methods.

A. FOM

This metric measures the displacement of the edge pixels between each filtered image f_{fil} and the reference image f_{ref}, establishing a map of edges for each image [9], [99]. The FoM is defined as:

$$FOM\left(f_{fil}, f_{ref}\right) = \frac{1}{max(N_{Filt}, N_{ref})} \sum_{i=1}^{\widehat{N}} \frac{1}{1 + d_i^2\, \alpha} \tag{54}$$

where N_{filt} and N_{ref} are the number of edge pixels in edge maps f_{fil} and f_{ref}, respectively; α is a constant (generally established as $1/9$); and d_i is the Euclidian distance of the i-th pixel between the filtered edge map and the reference edge map. The FoM can range between 0 and 1, where 1 represents a perfect preservation of the edge. The map is calculated using the most common Canny edge detector [100].

B. SSIM

The SSIM is used to evaluate the preservation of the structural information during the filtering process [101], and it is given by

$$SSIM = \frac{1}{M} \sum \frac{(2\mu_1 + C_1)(2\sigma_{12} + C_2)}{(\mu_1^2 + \mu_2^2 + C_1)(\sigma_1^2 + \sigma_2^2 + C_2)} \tag{55}$$

where μ_1, μ_2 and σ_1, σ_2 are the mean and the standard deviation of the images to be compared, and σ_{12} is the covariance between them. Such values are calculated using local statistics within a total of M windows, and their average is taken in (55). Constants $C_1, C_2 \ll 1$ ensure stability [101], and, in [9], they establish the size of M as 32. The values of SSIM range from 0 to 1, where 1 represents full structural similarity between images.

C. MSE

This metric measures the absolute averaged difference between two images as

$$MSE(f_{fil}, f_{orig}) = \frac{1}{XY} \sum_{i=1}^{Y} \sum_{j=1}^{X} (f_{fil}(x, y) - f_{orig}(x, y))^2 \tag{56}$$

where the images have the same size ($X \times Y$). Border Region MSE measures the averaged difference in the border areas considering only the pixels close to the edges of the image in (56). Several edge detection approaches are available, such as [102]–[106]. Nevertheless, this metric does not count spurious edges in images; instead, it considers all the edges that are sufficiently significant to be found by the implemented edge detector [9].

D. CNR

The CNR quantifies the contrast between an area of interest and the background, calculated as (57) [71]. Notwithstanding, in [107], the authors present five types of CNR metrics because their definitions include some measurement of the activation signal intensity, which can be differentiated depending on the activation signal amplitude and the standard deviation of the activation as the signal of interest.

$$CNR = \frac{\mu_1 - \mu_2}{\sqrt{\sigma_1^2 + \sigma_2^2}} \tag{57}$$

where μ_1 and σ_1^2 are the mean and variance of the intensity of the pixels in the region of interest, and μ_2 with σ_2^2 represent the mean and the variance of the intensity of the pixels in a region of the background of the image the same size as the region of interest.

E. SNR_A

In [107], [108], the level of speckle noise is calculated as the relationship between the mean and the standard deviation of the amplitude values.

$$SNR_A = \frac{\overline{S}}{\sigma_N} \tag{58}$$

where $\overline{S}$ and σ_N represent the mean of the signal and the standard deviation of noise, respectively.

F. NR QUALITY MEASUREMENTS

Perceptual quality is commonly evaluated in an empirical way using the mean of scores assigned by subjects who may be specialists in the field [109], [110]. However, such quality can also be assessed by algorithms. In particular, NR measurements quantify the perceptual quality of an image without depending on a reference image. Such measurements are commonly based on an estimated deviation from static natural images, as in [111]–[113]. In the latter, a perceptual quality index is proposed based on the Kullback-Leibler (KL) divergence between the distribution of the wavelet coefficients of $\hat{x}$ and those of the natural scenes. This idea was further expanded by popular methods such as DIIVINE [109], BRISQUE [110], BLIIND-II [114], and NIQE [115], which quantify perceptual quality employing several deviation measurements based on statistics of natural images in the spatial, wavelet, and cosine (DCT) domain [98].

Some studies [116]–[118] have already implemented several measures for speckle reduction applications. They have adopted what has been called blind assessment metrics (BAM), which include beta metric (β), speckle suppression index (SSI), speckle suppression, and mean preservation index (SMPI) [117]. The beta metric (β), according to [118], allows us to quantify the edge preservation capabilities of the despeckling algorithm, given as

$$\beta = \frac{\sum_{R,C}(\Delta f_o - \Delta\overline{f_o})(\Delta f_d - \Delta\overline{f_d})}{\sqrt{\sum_{R,C}(\Delta f_o - \Delta\overline{f_o})^2(\Delta f_d - \Delta\overline{f_d})^2}} \tag{59}$$

TABLE 1. Advantages and disadvantages of the categories considered in this work.

Techniques	Advantages	Disadvantages
Dynamic Analysis-Based Techniques	Gradual smoothing	Oversmoothing
	Strong speckle suppression	Exhaustive parameter tuning
		Removal of meaningful structural details with low-intensity contrasts.
SAR-Based Methods	Simple	Assumes Gaussian distribution
	Real-time implementations	Exhaustive parameter tuning (empirical)
	Good behavior in regions with constant distributions	Eradication of weak and diffused edges
		Poor performance if the variance of a region is quite high
Wavelet-Based Methods	Simple	Requires fine-tuning of thresholding value
	Properties like sparsity, multiresolution and multiscale nature	Tend to produce ringing artifacts when preserving features
	Good performance with high-level noise	
Modern Techniques (SBF)	Simple	Oversmoothing
	It very well preserves the local features	Introduce artifact
		Exhaustive parameter tuning
Modern Techniques (OBNLM)	Very efficient for smoothing homogeneous areas while preserving edges.	High complexity.
		Exhaustive parameter tuning.
		Features with low contrasts are usually heavily blurred.
Modern Techniques (SRBF)	Does not require a predefined region to tune the intensity of the filtering.	Introduce false edges
	It preserves the shape edge	Leads to staircase effect
		Gradient reversal
Hybrid Techniques	Good performance in speckle reduction.	Techniques are sensitive to the combination used.
	Edge preservation.	Increase the number of parameters to adjust.
	Achieves maintains important anatomical features.	It can be overfitting the type of US image used.
Machine Learning-Based Techniques	Avoid the manual fitting	High complexity
	generalize with different types of US data	Requires clean data for training

where Δf_o and Δf_d represent high-pass filtered versions of the original and filtered images, respectively; and $\Delta\overline{f_o}$ and $\Delta\overline{f_d}$ are the means of Δf_o and Δf_d, respectively.

In the case of SSI, $\sqrt{Var(f(x))}/Mean(f(x))$ is considered a measurement of speckle noise intensity over homogeneous areas; therefore, normalizing it to the original image $f(x)$, it is defined as

$$SSI = \frac{\sqrt{Var(\widehat{g})}}{Mean(\widehat{g})} \cdot \frac{Mean(f(x)}{\sqrt{Var(f(x))}}. \tag{60}$$

When SSI< 1.0, speckle noise is suppressed, which indicates that the lower the SSI, the greater the filter suppression capacity. In the cases where the filter overestimates the mean value, SSI is not reliable; therefore, SMPI is used. The equation is given as in [116].

$$SMPI = Q \cdot \frac{\sqrt{Var(\widehat{g})}}{\sqrt{Var(f(x))}} \tag{61}$$

And Q is calculated as follows:

$$Q = 1 + |mean(f(x)) - mean(\widehat{g})| \tag{62}$$

where lower values of SMPI indicate better performance of the filter in terms of mean preservation and noise reduction.

IX. CONCLUSION

This paper presented an overview of speckle noise filtering methods implemented in US images for improving the accuracy of their results, which has an impact on legal metrology for healthcare services focused on patient safety. The most common approaches in the field were described along with a group of new techniques and hybrid methods that have become very relevant in speckle filtering and offer new alternatives for solving common problems in US images.

Speckle filtering is usually neglected in subsequent stages (e.g., segmentation or detection of regions of interest) because it tends to smooth important features such as geometries and textures. Therefore, this study technically described a total of 27 different speckle filtering methods in US images, which were classified into dynamical analysis methods, time-frequency analyses, new methods, HT, and machine learning-based techniques. Moreover, five FR distortion metrics, common in filter evaluation processes, were detailed along with a methodology of compensation between FR and NR metrics, which can generate more certainty in the classification of the filters by taking into account information of the behavior in terms of perceptual quality, provided by the NR metrics.

It is noteworthy that Speckle filtering has different trends according to the groups in which it is analyzed, for example, in the diffusion group they have focused on looking for the function of diffusion coefficients that best allow the identification of edges, in order to separate regions that can be filtered from those that cannot (edges). Wavelet-based techniques focus on improving the way for finding a threshold that allows separating the coefficients that belong to the noise, in order for them to be filtered or eliminated. In the case of modern techniques, they seek to adapt classic methods of filtering images in general to the reduction of Speckle noise, by taking into account their multiplicative behavior and randomness, whose origin is due to the way that US images are generated. On the other hand, it should be noted that the Speckle reduction trend can continue in two fields: Hybrid Techniques and Machine Learning. On one hand, HT provide accurate results when Speckle is reduced, preserving important information, and these are based on identifying those methods that are compatible and a specific combination that exploits the advantages of each method used. However, such techniques are still based on the combination of classic and new techniques, which involves a manual fitting of parameters, as the response of such filters fluctuates depending on the type of input. Thus, the results of their implementation become subjective. In the case of machine learning-based techniques, these offer advantages compared to the manual fitting in other methods; nevertheless, they also present limitations as their training requires clean data that adequately represents the problem, which is difficult to generate in real situations and even more so for clinical cases.

The observations above and Table 1 can guide future research on speckle noise filtering in order to improve the detection of regions of interest and develop methodologies that offer better solutions to the problems previously described. Furthermore, the filter evaluation process should be enhanced, as more robust measurements of NR perceptual quality are required for real situations in which the ground truth is not available, such as in clinical cases. As a result, filter performance can be evaluated without any bias because, in most cases, it is calculated with FR distortion measurements and assessed with respect to the noisy image.

ACKNOWLEDGMENT

The authors would like to thank the Measurement Analysis & Decision Support Laboratory (AMYSOD Lab) and the Machine Intelligence & Pattern Recognition Laboratory (MIRP Lab) at Parque i, Instituto Tecnologico Metropolitano (ITM) in Medellin, Colombia.

REFERENCES

[1] R. Rosa and F. Monteiro, "Performance analysis of speckle ultrasound image filtering," *Comput. Methods Biomech. Biomed. Eng., Imag. Vis.*, vol. 4, pp. 1–9, Jul. 2014. [Online]. Available: http://www.tandfonline.com/doi/full/10.1080/21681163.2014.935803

[2] S. H. Contreras Ortiz, T. Chiu, and M. D. Fox, "Ultrasound image enhancement: A review," *Biomed. Signal Process. Control*, vol. 7, no. 5, pp. 419–428, Sep. 2012, doi: 10.1016/j.bspc.2012.02.002.

[3] J. Dainty, "Some statistical properties of random speckle patterns in coherent and partially coherent illumination," *Optica Acta, Int. J. Opt.*, vol. 17, no. 10, pp. 761–772, Oct. 1970.

[4] J. W. Goodman, "Some fundamental properties of speckle," *J. Opt. Soc. Amer.*, vol. 66, no. 11, pp. 1145–1150, Nov. 1976.

[5] K. Singh, S. K. Ranade, and C. Singh, "A hybrid algorithm for speckle noise reduction of ultrasound images," *Comput. Methods Programs Biomed.*, vol. 148, pp. 55–69, Sep. 2017. [Online]. Available: http://linkinghub.elsevier.com/retrieve/pii/S0169260717301979

[6] J. Zhang, C. Wang, and Y. Cheng, "Comparison of despeckle filters for breast ultrasound images," *Circuits Syst. Signal Process.*, vol. 34, no. 1, pp. 185–208, Jan. 2015.

[7] A. Thakur and R. Anand, "Image quality based comparative evaluation of wavelet filters in ultrasound speckle reduction," *Digit. Signal Process.*, vol. 15, no. 5, pp. 455–465, Sep. 2005.

[8] A. Fernández-Caballero and J. M. Vega-Riesco, "Determining heart parameters through left ventricular automatic segmentation for heart disease diagnosis," *Expert Syst. Appl.*, vol. 36, no. 2, pp. 2234–2249, Mar. 2009.

[9] S. Finn, M. Glavin, and E. Jones, "Echocardiographic speckle reduction comparison," *IEEE Trans. Ultrason., Ferroelectr., Freq. Control*, vol. 58, no. 1, pp. 82–101, Jan. 2011.

[10] J. Jensen, "Simulation of advanced ultrasound systems using Field II," in *Proc. 2nd IEEE Int. Symp. Biomed. Imag., Nano Macro*, Apr. 2004, pp. 636–639.

[11] A. Kapoor and T. Singh, "A brief review: Speckle reducing filtering for ultrasound images," in *Proc. Int. Conf. I-SMAC (IoT Social, Mobile, Anal. Cloud)(I-SMAC)*, 2017, pp. 242–246.

[12] V. Damerjian, O. Tankyevych, N. Souag, and E. Petit, "Speckle characterization methods in ultrasound images—A review," *IRBM*, vol. 35, no. 4, pp. 202–213, Sep. 2014. [Online]. Available: http://linkinghub.elsevier.com/retrieve/pii/S1959031814000797, doi: 10.1016/j.irbm.2014.05.003.

[13] C. P. Loizou and C. S. Pattichis, "Despeckle filtering of ultrasound images," in *Atherosclerosis Disease Management*. New York, NY, USA: Springer, 2011, ch. 7, p. 153.

[14] A. K. Jain, "Digital processing of speckle images," in *Fundamentals of Digital Image Processing*. Englewood Cliffs, NJ, USA: Prentice-Hall, 1989, ch. 8.

[15] X. Zong, A. F. Laine, and E. A. Geiser, "Speckle reduction and contrast enhancement of echocardiograms via multiscale nonlinear processing," *IEEE Trans. Med. Imag.*, vol. 17, no. 4, pp. 532–540, Aug. 1998. [Online]. Available: http://ieeexplore.ieee.org/document/730398/

[16] K. Abd-Elmoniem, A.-B. Youssef, and Y. Kadah, "Real-time speckle reduction and coherence enhancement in ultrasound imaging via nonlinear anisotropic diffusion," *IEEE Trans. Biomed. Eng.*, vol. 49, no. 9, pp. 997–1014, Sep. 2002.

[17] R. Wagner, S. Smith, J. Sandrik, and H. Lopez, "Statistics of speckle in ultrasound B-scans," *IEEE Trans. Son. Ultrason.*, vol. 30, no. 3, pp. 156–163, May 1983.

[18] M. F. Insana, R. F. Wagner, B. S. Garra, D. V. Brown, and S. H. Shawker, "Analysis of ultrasound image texture via generalized Rician statistics," in *Proc. Int. Conf. Speckle*, vol. 556, 1985, p. 7.

[19] P. Mohana Shankar, "A general statistical model for ultrasonic backscattering from tissues," *IEEE Trans. Ultrason., Ferroelectr., Freq. Control*, vol. 47, no. 3, pp. 727–736, May 2000.

[20] B. Raju and M. Srinivasan, "Statistics of envelope of high-frequency ultrasonic backscatter from human skin *in vivo*," *IEEE Trans. Ultrason., Ferroelectr., Freq. Control*, vol. 49, no. 7, pp. 871–882, Jul. 2002.

[21] D. Fernandes and M. Sekine, *Suppression Weibull Radar Clutter*, vol. E76-B, no. 10. Tokyo, Japan: Institute of Electronics, Information and Communication Engineers, 1993. [Online]. Available: https://search.ieice.org/bin/summary.php?id=e76-b_10_1231

[22] S. M. Kay, *Fundamentals of Statistical Signal Processing: Estimation Theory*, vol. 1. Upper Saddle River, NJ, USA: Prentice-Hall, 1993.

[23] S. Balocco, C. Gatta, O. Pujol, J. Mauri, and P. Radeva, "SRBF: Speckle reducing bilateral filtering," *Ultrasound Med. Biol.*, vol. 36, no. 8, pp. 1353–1363, Aug. 2010.

[24] K. Dabov, A. Foi, and V. Katkovnik, "Image denoising by sparse 3D transformation-domain collaborative filtering," *IEEE Trans. Image Process.*, vol. 16, no. 8, pp. 2080–2095, Aug. 2007. [Online]. Available: http://ieeexplore.ieee.org/stamp/stamp.jsp?tp=&arnumber=4271520

[25] D. Kalplan and Q. Ma, "On the statistical characteristics of the log-compressed Rayleigh signals," in *Proc. Ultrason. Symp.*, vol. 961, 1993, pp. 961–964.

[26] J. Bamber and C. Daft, "Adaptive filtering for reduction of speckle in ultrasonic pulse-echo images," *Ultrasonics*, vol. 24, no. 1, pp. 41–44, Jan. 1986.

[27] C. P. Loizou, *Despeckle Filtering for Ultrasound Imaging and Video* (Synthesis Lectures on Algorithms and Software in Engineering), A. Spanias, Ed., 2nd ed. Williston, VT, USA: Morgan & Claypool, 2015.

[28] C. Lopez-Molina, J. Montero, H. Bustince, and B. De Baets, "Gradient funsion operator for vector-valued image processing," in *Proc. 10th Conf. Eur. Soc. Fuzzy Logic Technol. Adv. Fuzzy Logic Technol. (EUSFLAT)*, 2017, pp. 430–442.

[29] C. Lopez-Molina, M. Galar, H. Bustince, and B. De Baets, "On the impact of anisotropic diffusion on edge detection," *Pattern Recognit.*, vol. 47, no. 1, pp. 270–281, Jan. 2014, doi: 10.1016/j.patcog.2013.07.009.

[30] P. Perona and J. Malik, "Scale-space and edge detection using anisotropic diffusion," *IEEE Trans. Pattern Anal. Mach. Intell.*, vol. 12, no. 7, pp. 629–639, Jul. 1990.

[31] Y. Yongjian and S. T. Acton, "Deconvolutional speckle reducing anisotropic diffusion," in *Proc. Int. Conf. Image Process. (ICIP)*, 2002, vol. 1, no. 11, pp. 5–8.

[32] S. Aja-Fernandez and C. Alberola-Lopez, "On the estimation of the coefficient of variation for anisotropic diffusion speckle filtering," *IEEE Trans. Image Process.*, vol. 15, no. 9, pp. 2694–2701, Sep. 2006.

[33] Y. Yu and S. Acton, "Edge detection in ultrasound imagery using the instantaneous coefficient of variation," *IEEE Trans. Image Process.*, vol. 13, no. 12, pp. 1640–1655, Dec. 2004.

[34] J. Weickert, "Coherence-enhancing diffusion filtering," *Int. J. Comput. Vis.*, vol. 31, no. 2, pp. 111–127, 1999. [Online]. Available: http://www.springerlink.com/content/q7kr7v15n8437021/

[35] K. Krissian, C.-F. Westin, R. Kikinis, and K. G. Vosburgh, "Oriented speckle reducing anisotropic diffusion," *IEEE Trans. Image Process.*, vol. 16, no. 5, pp. 1412–1424, May 2007.

[36] K. Krissian, "Flux-based anisotropic diffusion applied to enhancement of 3-D angiogram," *IEEE Trans. Med. Imag.*, vol. 21, no. 11, pp. 1440–1442, Nov. 2002.

[37] J. Xu, Y. Jia, Z. Shi, and K. Pang, "An improved anisotropic diffusion filter with semi-adaptive threshold for edge preservation," *Signal Process.*, vol. 119, pp. 80–91, Feb. 2016, doi: 10.1016/j.sigpro.2015.07.017.

[38] J. Joseph and R. Periyasamy, "A polynomial model for the adaptive computation of threshold of gradient modulus in 2D anisotropic diffusion filter," *Optik*, vol. 157, pp. 841–853, Mar. 2018, doi: 10.1016/j.ijleo.2017.11.177.

[39] H. K. Rafsanjani, M. H. Sedaaghi, and S. Saryazdi, "An adaptive diffusion coefficient selection for image denoising," *Digit. Signal Process., Rev. J.*, vol. 64, pp. 71–82, May 2017, doi: 10.1016/j.dsp.2017.02.004.

[40] J. Joseph and R. Periyasamy, "An analytical method for the adaptive computation of threshold of gradient modulus in 2D anisotropic diffusion filter," *Optik*, vol. 157, no. 1, pp. 841–853, 2018. [Online]. Available: http://dx.doi.org/10.1016/j.bbe.2016.12.002

[41] H. Guo, J. E. Odegard, M. Lang, R. A. Gopinath, I. W. Selesnick, and C. S. Burrus, "Wavelet based speckle reduction with application to SAR based ATD/R," in *Proc. 1st Int. Conf. Image Process.*, 1994, vol. 1, no. 2, pp. 75–79.

[42] S. Mallat and S. Zhong, "Characterization of signals from multiscale edges," *IEEE Trans. Pattern Anal. Mach. Intell.*, vol. 14, no. 7, pp. 710–732, Jul. 1992.

[43] S. Gupta, R. C. Chauhan, and S. C. Sexana, "A wavelet based statistical approach for speckle reduction in medical ultrasound images," *Med. Biol. Eng. Comput.*, vol. 42, no. 1976, pp. 189–192, 2004.

[44] Y. Yue, M. Croitoru, A. Bidani, J. Zwischenberger, and J. Clark, "Nonlinear multiscale wavelet diffusion for speckle suppression and edge enhancement in ultrasound images," *IEEE Trans. Med. Imag.*, vol. 25, no. 3, pp. 297–311, Mar. 2006.

[45] A. Pizurica, W. Philips, I. Lemahieu, and M. Acheroy, "A versatile wavelet domain noise filtration technique for medical imaging," *IEEE Trans. Med. Imag.*, vol. 22, no. 3, pp. 323–331, Mar. 2003.

[46] C. Vimalraj, S. Esakkirajan, T. Veerakumar, and P. Sreevidya, "Direction sensitive wavelet packet for despeckling of ultrasound images," *IET Comput. Vis. J.*, vol. 10, no. 7, pp. 746–757, Oct. 2016.

[47] S. Esakkirajan, C. T. Vimalraj, R. Muhammed, and G. Subramanian, "Adaptive wavelet packet-based de-speckling of ultrasound images with bilateral filter," *Ultrasound Med. Biol.*, vol. 39, no. 12, pp. 2463–2476, Dec. 2013.

[48] A. Currie, "Synthetic aperture radar," *Electron. Commun. Eng. J.*, vol. 3, no. 4, pp. 1–23, 1991.

[49] J. S. Lee, "Digital image enhancement and noise filtering by use of local statistics," *IEEE Trans. Pattern Anal. Mach. Intell.*, vol. PAMI-2, no. 2, pp. 165–168, Feb. 1980.

[50] A. K. Jain, *Fundamentals of Digital Image Processing*, vol. 46, no. 3. Englewood Cliffs, NJ, USA: Prentice-Hall, 1989. [Online]. Available: http://linkinghub.elsevier.com/retrieve/pii/0734189X89900418

[51] D. Kuan, A. Sawchuk, T. Strand, and P. Chavel, "Adaptive restoration of images with speckle," *IEEE Trans. Acoust., Speech, Signal Process.*, vol. ASSP-35, no. 3, pp. 373–383, Mar. 1987.

[52] A. Baraldi and F. Parmiggiani, "An alternative form of the lee filter for speckle suppression in SAR images," *Graph. Models Image Process.*, vol. 57, pp. 75–78, Jan. 1995. [Online]. Available: http://www.scopus.com/inward/record.url?eid=2-s2.0-0029210168&partnerID=40&md5=db6866a73d2f34ba1499e49e8f3c36a6

[53] V. S. Frost, J. A. Stiles, K. S. Shanmugan, and J. C. Holtzman, "A model for radar images and its application to adaptive digital filtering of multiplicative noise," *IEEE Trans. Pattern Anal. Mach. Intell.*, vol. 4, no. 2, pp. 157–166, 1982.

[54] A. Lopes, R. Touzi, and E. Nezry, "Adaptive speckle filters and scene heterogeneity," *IEEE Trans. Geosci. Remote Sens.*, vol. 28, no. 6, pp. 992–1000, Nov. 1990.

[55] P. C. Tay, C. D. Garson, S. T. Acton, and J. A. Hossack, "Ultrasound despeckling for contrast enhancement," *IEEE Trans. Image Process.*, vol. 19, no. 7, pp. 1847–1860, Jul. 2010.
[56] L. Zhu, W. Wang, J. Qin, K.-H. Wong, K.-S. Choi, and P.-A. Heng, "Fast feature-preserving speckle reduction for ultrasound images via phase congruency," *Signal Process.*, vol. 134, pp. 275–284, May 2017, doi: 10.1016/j.sigpro.2016.12.011.
[57] T. Aysal and K. Barner, "Rayleigh-maximum-likelihood filtering for speckle reduction of ultrasound images," *IEEE Trans. Med. Imag.*, vol. 26, no. 5, pp. 712–727, May 2007.
[58] C. Tomasi and R. Manduchi, "Bilateral filtering for gray and color images," in *Proc. 6th Int. Conf. Comput. Vis.*, vol. 6, 1998, pp. 839–846. [Online]. Available: http://ieeexplore.ieee.org/document/710815/
[59] M. Elad, "On the origin of the bilateral filter and ways to improve it," *IEEE Trans. Image Process.*, vol. 11, no. 10, pp. 1141–1151, Oct. 2002.
[60] A. Buades, B. Coll, J.-M. Morel, and J.-M. M. A., "A review of image denoising algorithms, with a new one," *J. Multiscale Model. Simul.*, vol. 4, no. 2, pp. 490–530, 2005.
[61] P. Coupe, P. Hellier, C. Kervrann, and C. Barillot, "Nonlocal means-based speckle filtering for ultrasound images," *IEEE Trans. Image Process.*, vol. 18, no. 10, pp. 2221–2229, Oct. 2009.
[62] P. Coupe, P. Yger, S. Prima, P. Hellier, C. Kervrann, and C. Barillot, "An optimized blockwise nonlocal means denoising filter for 3-D magnetic resonance images," *IEEE Trans. Med. Imag.*, vol. 27, no. 4, pp. 425–441, Apr. 2008.
[63] J. E. Odegard, H. Guo, M. Lang, C. S. Burrus, R. O. Wells, L. M. Novak, and M. Hiett, "Wavelet-based SAR speckle reduction and image compression," *Proc. SPIE*, vol. 2487, pp. 259–271, Jun. 1995.
[64] L. Gagnon and F. D. Smaili, "Speckle noise reduction of airborne SAR images with symmetric Daubechies wavelets," *Proc. SPIE*, vol. 2759, pp. 14–24, May 1996. [Online]. Available: http://proceedings.spiedigitallibrary.org/proceeding.aspx?articleid=1019052
[65] Z. Tao, H. Tagare, and J. Beaty, "Evaluation of four probability distribution models for speckle in clinical cardiac ultrasound images," *IEEE Trans. Med. Imag.*, vol. 25, no. 11, pp. 1483–1491, Nov. 2006.
[66] G. Slabaugh, G. Unal, F. Tong, and M. Wels, "Ultrasound-specific segmentation via decorrelation and statistical region-based active contours," in *Proc. IEEE Comput. Soc. Conf. Comput. Vis. Pattern Recognit.*, vol. 1, Jun. 2006, pp. 45–52.
[67] T. Loupas, W. McDicken, and P. Allan, "An adaptive weighted median filter for speckle suppression in medical ultrasound image," *IEEE Trans. Circuits Syst.*, vol. 36, no. 1, pp. 129–135, Jan. 1989.
[68] H. Xiaohui, G. Shangkai, and G. Xiaorong, "A novel multiscale nonlinear thresholding method for ultrasonic speckle suppressing," *IEEE Trans. Med. Imag.*, vol. 18, no. 9, pp. 94–787, Sep. 1999. [Online]. Available: http://www.ncbi.nlm.nih.gov/pubmed/10571383
[69] K. Krissian, R. Kikinis, C. F. Westin, and K. Vosburgh, "Speckle constrained filtering of ultrasound images," in *Proc. IEEE Comput. Soc. Conf. Comput. Vis. Pattern Recognit. (CVPR)*, Jun. 2005, vol. 6, no. 1, pp. 547–552.
[70] F. Argenti and G. Torricelli, "Speckle suppression in ultrasonic images based on undecimated wavelets," *EURASIP J. Appl. Signal Process.*, vol. 2003, no. 5, pp. 470–478, 2003.
[71] Y. Zhan, M. Ding, L. Wu, and X. Zhang, "Nonlocal means method using weight refining for despeckling of ultrasound images," *Signal Process.*, vol. 103, pp. 201–213, Oct. 2014, doi: 10.1016/j.sigpro.2013.12.019.
[72] K. He, J. Sun, and X. Tang, "Guided image filtering," *IEEE Trans. Pattern Anal. Mach. Intell.*, vol. 35, no. 6, pp. 409–1397, Jun. 2013. [Online]. Available: http://www.ncbi.nlm.nih.gov/pubmed/24110615
[73] H. Choi and J. Jeong, "Despeckling images using a preprocessing filter and discrete wavelet transform-based noise reduction techniques," *IEEE Sensors J.*, vol. 18, no. 8, pp. 3131–3139, Apr. 2018.
[74] J. V. Manjón, P. Coupé, A. Buades, D. Louis Collins, and M. Robles, "New methods for MRI denoising based on sparseness and self-similarity," *Med. Image Anal.*, vol. 16, no. 1, pp. 18–27, Jan. 2012.
[75] J. Yang, J. Fan, D. Ai, X. Wang, Y. Zheng, S. Tang, and Y. Wang, "Local statistics and non-local mean filter for speckle noise reduction in medical ultrasound image," *Neurocomputing*, vol. 195, pp. 88–95, Jun. 2016, doi: 10.1016/j.neucom.2015.05.140.
[76] D. T. Kuan, A. A. Sawchuk, T. C. Strand, and P. Chavel, "Adaptive noise smoothing filter for images with signal-dependent noise," *IEEE Trans. Pattern Anal. Mach. Intell.*, vol. PAMI-7, no. 2, pp. 165–177, Mar. 1985.
[77] N. Ahmed, "A hybrid technique for speckle noise reduction in ultrasound images," Ph.D. dissertation, Sudan Univ. Sci. Technol., Khartoum, Sudan, 2016.
[78] S. G. Mallat, "A theory for multiresolution signal decomposition: The wavelet representation," *IEEE Trans. Pattern Anal. Mach. Intell.*, vol. 7, no. 11, pp. 674–693, Jul. 1989.
[79] R. Vanithamani, G. Umamaheswari, and M. Ezhilarasi, "Modified hybrid median filter for effective speckle reduction in ultrasound images," *Recent Adv. Netw., VLSI Signal Process.*, no. 1, pp. 166–171, 2010.
[80] C.-C. Lai and C.-C. Tsai, "Digital image watermarking using discrete wavelet transform and singular value decomposition," *IEEE Trans. Instrum. Meas.*, vol. 59, no. 11, pp. 3060–3063, Nov. 2010.
[81] L. I. Rudin, S. Osher, and E. Fatemi, "Nonlinear total variation based noise removal algorithms," *Phys. D, Nonlinear Phenomena*, vol. 60, nos. 1–4, pp. 259–268, Nov. 1992.
[82] V. N. P. Raj and T. Venkateswarlu, "Denoising of medical images using total variational method," *Signal Image Process., Int. J.*, vol. 3, no. 2, pp. 131–142, 2012.
[83] S. Vedula, O. Senouf, A. M. Bronstein, O. V. Michailovich, and M. Zibulevsky, "Towards CT-quality ultrasound imaging using deep learning," 2017, *arXiv:1710.06304*. [Online]. Available: https://arxiv.org/abs/1710.06304
[84] O. V. Michailovich and A. Tannenbaum, "Despeckling of medical ultrasound images," *IEEE Trans. Ultrason., Ferroelectr., Freq. Control*, vol. 53, no. 1, pp. 64–78, Jan. 2006.
[85] O. Kutter, R. Shams, and N. Navab, "Visualization and GPU-accelerated simulation of medical ultrasound from CT images," *Comput. Methods Programs Biomed.*, vol. 94, no. 3, pp. 250–266, Jun. 2009.
[86] Frederick National Laboratory for Cancer Research. (2018). *The Cancer Imaging Archive (TCIA)*. [Online]. Available: http://www.cancerimagingarchive.net/
[87] D. Mishra, S. Tyagi, S. Chaudhury, and M. Sarkar, "Despeckling CNN with ensembles of classical outputs," in *Proc. Int. Conf. Pattern Recognit. (ICPR)*, 2018, pp. 3802–3807.
[88] M. V. Hernández, V. González-castro, S. Diniz, J. Barbosa, P. Chen, X. Du, J. Filipe, O. Kara, I. Kotenko, T. Liu, K. M. Sivalingam, and T. Washio, "Medical image understanding and analysis," *Med. Image Understand. Anal.*, vol. 894, no. 21, pp. 109–120, 2017. [Online]. Available: http://link.springer.com/10.1007/978-3-319-95921-4
[89] G. Ramos-Llorden, G. Vegas-Sanchez-Ferrero, M. Martin-Fernandez, C. Alberola-Lopez, and S. Aja-Fernandez, "Anisotropic diffusion filter with memory based on speckle statistics for ultrasound images," *IEEE Trans. Image Process.*, vol. 24, no. 1, pp. 345–358, Jan. 2015.
[90] H. Zhao, O. Gallo, I. Frosio, and J. Kautz, "Loss functions for image restoration with neural networks," *IEEE Trans. Comput. Imag.*, vol. 3, no. 1, pp. 47–57, Mar. 2017.
[91] D. Mishra, S. Chaudhury, M. Sarkar, and A. S. Soin, "Ultrasound image enhancement using structure oriented adversarial network," *IEEE Signal Process. Lett.*, vol. 25, no. 9, pp. 1349–1353, Sep. 2018.
[92] C. Perreault and M.-F. Auclair-Fortier, "Speckle simulation based on B-mode echographic image acquisition model," in *Proc. 4th Can. Conf. Comput. Robot. Vis.*, 2007, pp. 379–386.
[93] M. Tanter and M. Fink, "Ultrafast imaging in biomedical ultrasound," *IEEE Trans. Ultrason., Ferroelectr., Freq. Control*, vol. 61, no. 1, pp. 102–119, Jan. 2014.
[94] M. Gasse, F. Millioz, E. Roux, D. Garcia, H. Liebgott, and D. Friboulet, "High-quality plane wave compounding using convolutional neural networks," *IEEE Trans. Ultrason., Ferroelectr., Freq. Control*, vol. 64, no. 10, pp. 1637–1639, Oct. 2017.
[95] D. Perdios, M. Vonlanthen, A. Besson, F. Martinez, M. Arditi, and J.-P. Thiran, "Deep Convolutional Neural Network for Ultrasound Image Enhancement," in *Proc. IEEE Int. Ultrason. Symp. (IUS)*, Oct. 2018, pp. 1–4.
[96] S. Finn, E. Jones, and M. Glavin, "Objective and subjective evaluations of quality for speckle reduced echocardiography," in *Proc. 31st Annu. Int. Conf. IEEE Eng. Med. Biol. Soc., Eng. Future Biomed. (EMBC)*, Sep. 2009, pp. 503–506.
[97] C. I. Gonzalez, P. Melin, J. R. Castro, O. Mendoza, and O. Castillo, "An improved sobel edge detection method based on generalized type-2 fuzzy logic," *Soft Comput.*, vol. 20, no. 2, pp. 773–784, Feb. 2016.
[98] Y. Blau and T. Michaeli, "The perception-distortion tradeoff," in *Proc. Comput. Vis. Pattern Recognit. (CVPR)*, 2018, pp. 6228–6237. [Online]. Available: http://arxiv.org/abs/1711.06077

[99] I. E. Abdou and W. K. Pratt, "Quantitative design and evaluation of enhancement/thresholding edge detectors," *Proc IEEE*, vol. 67, no. 5, pp. 753–763, May 1979.

[100] J. Canny, "A computational approach to edge detection," *IEEE Trans. Pattern Anal. Mach. Intell.*, vol. PAMI-8, no. 6, pp. 679–698, Nov. 1986.

[101] Z. Wang, A. Bovik, H. Sheikh, and E. Simoncelli, "Image quality assessment: From error visibility to structural similarity," *IEEE Trans. Image Process.*, vol. 13, no. 4, pp. 600–612, Apr. 2004.

[102] A. Bovik, "On detecting edges in speckle imagery," *IEEE Trans. Acoust., Speech, Signal Process.*, vol. ASSP-36, no. 10, pp. 1618–1627, Oct. 1988.

[103] R. Czerwinski, D. Jones, and W. J. O'Brien, "Edge detection in ultrasound speckle noise," in *Proc. IEEE Int. Conf.*, vol. 3, Nov. 1994, pp. 304–308.

[104] C. Oliver, D. Blacknell, and R. White, "Optimum edge detection in SAR," *IEE Proc.-Radar, Sonar Navigat.*, vol. 143, no. 1, p. 31, 1996. [Online]. Available: http://digital-library.theiet.org/content/journals/10.1049/ip-rsn_19960219

[105] C. Oliver and P. Lombardo, "Simultaneous mean and texture edge detection in SAR clutter," *IEE Proc.-Radar, Sonar Navigat.*, vol. 143, no. 6, p. 391, 1996. [Online]. Available: http://link.aip.org/link/IRSNE2/v143/i6/p391/s1&Agg=doi

[106] R. Touzi, A. Lopes, and P. Bousquet, "A statistical and geometrical edge detector for SAR images," *IEEE Trans. Geosci. Remote Sens.*, vol. GRS-26, no. 6, pp. 764–773, Nov. 1988.

[107] M. Welvaert and Y. Rosseel, "On the definition of signal-to-noise ratio and contrast-to-noise ratio for fMRI data," *PLoS ONE*, vol. 8, no. 11, Nov. 2013, Art. no. e77089.

[108] C. B. Burckhardt, "Speckle in ultrasound B-mode scans," *IEEE Trans. Sonics Ultrason.*, vol. SU-25, no. 1, pp. 1–6, Jan. 1978.

[109] A. K. Moorthy and A. C. Bovik, "Blind image quality assessment: From natural scene statistics to perceptual quality," *IEEE Trans. Image Process.*, vol. 20, no. 12, pp. 3350–3364, Dec. 2011.

[110] A. Mittal, A. K. Moorthy, and A. C. Bovik, "No-reference image quality assessment in the spatial domain," *IEEE Trans. Image Process.*, vol. 21, no. 12, pp. 4695–4708, Dec. 2012.

[111] Q. Li and Z. Wang, "Reduced-reference image quality assessment using divisive normalization-based image representation," *IEEE J. Sel. Top. Signal Process.*, vol. 3, no. 2, pp. 202–211, Apr. 2009.

[112] Z. Wang and E. P. Simoncelli, "Reduced-reference image quality assessment using a wavelet-domain natural image statistic model," *Hum. Vis. Electron. Imag.*, vol. 5666, no. 18, pp. 149–159, 2005.

[113] Z. Wang, G. Wu, H. Sheikh, E. Simoncelli, E.-H. Yang, and A. Bovik, "Quality-aware images," *IEEE Trans. Image Process.*, vol. 15, no. 6, pp. 1680–1689, Jun. 2006.

[114] M. A. Saad, A. C. Bovik, and C. Charrier, "Blind image quality assessment: A natural scene statistics approach in the DCT domain," *IEEE Trans. Image Process.*, vol. 21, no. 8, pp. 3339–3352, Aug. 2012.

[115] A. Mittal, R. Soundararajan, and A. C. Bovik, "Making a 'completely blind' image quality analyzer," *IEEE Signal Process. Lett.*, vol. 20, no. 3, pp. 209–212, Nov. 2013.

[116] X. Wang, L. Ge, and L. Xiaojing, "Evaluation of filters for ENVISAT ASAR speckle suppression in pasture area," *ISPRS Ann. Photogramm., Remote Sens. Spatial Inf. Sci.*, vol. 1, pp. 341–346, Sep. 2012.

[117] N. Biradar, M. L. Dewal, M. Rohit, S. Gowre, and Y. Gundge, "Blind source parameters for performance evaluation of despeckling filters," *Int. J. Biomed. Imag.*, vol. 2016, pp. 1–12, 2016.

[118] Kriti, J. Virmani, and R. Agarwal, "Assessment of despeckle filtering algorithms for segmentation of breast tumours from ultrasound images," *Biocybern. Biomed. Eng.*, vol. 39, no. 1, pp. 100–121, Jan. 2019, doi: 10.1016/j.bbe.2018.10.002.

CARLOS A. DUARTE-SALAZAR received the B.S. degree in biomedical engineering from the Instituto Tecnológico Metropolitano (ITM), Medellin, Colombia, in 2016, where he is currently pursuing the master's degree in automation and industrial control. His research interests include image preprocessing, machine learning, and computer vision.

ANDRÉS EDUARDO CASTRO-OSPINA received the bachelor's degree in electronic engineering and the master's degree in industrial automation from the Universidad Nacional de Colombia Sede Manizales, in 2011 and 2014, respectively. He is currently an Auxiliar Professor with the Instituto Tecnológico Metropolitano, Medellin. His research interests include machine learning and pattern recognition oriented to biomedical applications.

MIGUEL A. BECERRA received the bachelor's degree in electronic engineering from the Universidad Nacional de Colombia, in 2002, the master's degree in virtuality pedagogy, in 2008, and the master's degree in industrial automation and control, in 2012. He is currently pursuing the Ph.D. degree with UdeM. He is currently a Professor with the Institución Universitaria Pascual Bravo, Medellín. His research interests include data fusion, information quality, and signal processing.

EDILSON DELGADO-TREJOS (Member, IEEE) received the B.S. degree in electronic engineering, the M.S. degree in industrial automation, and the Ph.D. degree in engineering sciences from the Universidad Nacional de Colombia, in 2000, 2003, and 2008, respectively. Since August 2008, he has been a full-time Lecturer and a Senior Researcher with the Instituto Tecnológico Metropolitano (ITM), Medellin, Colombia. He is currently an Associate Professor and a Vice-Chancellor of Research and Academic Extension ITM. He has published more than 50 articles, ten book chapters, and three books in indexed scientific journals and editorials. His current research interests include pattern recognition, machine learning, multivariate data analysis, nonlinear analysis, signal processing, and soft metrology.